Origin of the band gap in Bi-intercalated graphene on Ir(111)

M. Krivenkov[1,2], D. Marchenko[1], J. Sánchez-Barriga[1], E. Golias[1], O. Rader[1] and A. Varykhalov[1,*]
[1] *Helmholtz-Zentrum Berlin für Materialien und Energie, Elektronenspeicherring BESSY II, Albert-Einstein-Str. 15, 12489 Berlin, Germany*
[2] *Institut für Physik und Astronomie, Universität Potsdam, Karl-Liebknecht-Str. 24/25, 14476 Potsdam, Germany and*
[*] *Corresponding author: andrei.varykhalov@helmholtz-berlin.de*

Proximity to heavy *sp*-elements is considered promising for reaching a band gap in graphene that could host quantum spin Hall states. The recent report of an induced spin-orbit gap of 0.2 eV in Pb-intercalated graphene detectable by spin-resolved photoemission has spurred renewed interest in such systems [ACS Nano **11**, 368 (2017)]. In the case of Bi intercalation an even larger band gap of 0.4 eV has been observed but was assigned to the influence of a dislocation network [Phys. Rev. B **93**, 165437 (2016)]. Here, we study Bi intercalation under graphene on Ir(111) and report a nearly ideal graphene dispersion without band replicas and no indication of hybridization with the substrate. The band gap is small (0.19 eV) and can be tuned by ±25 meV through the Bi coverage. The Bi atomic density is higher than in the recent report. By spin-resolved photoemission we exclude induced spin-orbit interaction as origin of the gap. Quantitative agreement of a photoemission intensity analysis with the measured band gap suggests sublattice symmetry breaking as one of the possible band gap opening mechanisms. We test several Bi structures by density functional theory. Our results indicate the possibility that Bi intercalates in the phase of bismuthene forming a graphene-bismuthene van der Waals heterostructure.

PACS numbers: 73.22.Pr, 61.48.Gh, 68.65.Pq

I. INTRODUCTION

Intercalation of epitaxial graphene with foreign chemical elements has been in the spotlight of physics research for a decade. It has established itself as a universal method for the creation of epitaxial interfaces between graphene and various materials. The variety of substrates on which epitaxial graphene can be grown directly (e.g. by thermal depletion of the constituents and by chemical vapour deposition) is limited. The most widely used ones are silicon carbide [1–3] and transition metals [4] able to provide high quality graphene crystals.

On the other hand, intercalation of foreign species between graphene and its substrate allows realization of interfaces to a much more versatile set of materials, including noble metals [5–7], antiferromagnetics [8], semiconductors [9, 10] and even fullerene molecules [11]. Engineering of such interfaces permits to control charge doping and energy gap of Dirac bands in graphene in a very flexible way.

Of particular interest are heavy elements due to their high spin-orbit interaction. While heavy *sp*-metals Tl and In have been suggested for realizing the quantum spin Hall effect in graphene [12], the presence of d-states in the valence band favor a Rashba-type spin-orbit interaction [7, 13–15]. In such a way, a Rashba-type splitting of the Dirac cone [16] ranging from 13 to 100 meV has been achieved in Au-intercalated graphene on Ni(111) [6, 7]. Recently, the giant value of such spin-orbit splitting was explained by the enhancement of graphene-Au hybridization due to periodic stapling of graphene on arrays of intercalated Au nanoparticles [17]. Particularly important in these systems is the band gap at the Dirac point as it can lead to the out-of-plane spin polarization [18] as it was shown for intercalated Au [19]. A spin polarization in the gap was also shown for intercalated Pb [20]. While sublattice symmetry breaking in graphene/Au/Fe(110) leads to a band gap in which the Rashba-type spin polarization turns out of the surface plane [19], the gap in graphene/Pb/Pt(111) is assigned predominantly to intrinsic spin-orbit interaction [20]. This is very interesting since it could enable the quantum spin Hall effect [12, 21].

In the present article we study the structural and electronic properties of epitaxial graphene on Ir(111) intercalated with *sp*-metal Bi. The study has been performed with angle- and spin-resolved photoelectron spectroscopy (ARPES) and scanning tunneling microscopy (STM). We observe a much smaller band gap at the Dirac point than recently reported by Warmuth et al. for this intercalation system [22]. Extensive characterization by ARPES and STM reveals that we achieve a novel intercalation phase characterized by high density of intercalated Bi which is strikingly different from the phase reported by Warmuth et al. which we refer to as low-density (LD) phase.

The low-density phase of Bi-intercalated graphene [22] contains only 0.3 monolayer (ML) of Bi arranged in a $(\sqrt{3} \times \sqrt{3})$ $R30°$ superstructure and reveals a strong perturbation of the graphene symmetry and a large band gap at the Dirac point ($E_g \sim 0.42$ eV). In contrast, the phase reported here [referred to in the following as high-density (HD) phase] contains much higher concentration of intercalated Bi. Moreover, the thickness of the Bi interlayer can, according to our STM measurements, exceed a single atomic layer and reach up to 3 ML. Interlayer of Bi enables

nearly unperturbed quasifreestanding graphene with much narrower band gap E_g <0.2 eV and no contributions from the Ir substrate to the photoemission signal due to the high Bi density. We show that the HD-phase allows fine tuning ($\pm$25 meV) of the band gap E_g through the Bi concentration. We also study its effect on the electronic hybridization between graphene and Ir(111), Ir-induced quantum-size effects as well as the Ir(111) surface state and demonstrate the complete suppression of all these features.

By performing spin-resolved ARPES we exclude bismuth-induced spin-orbit interaction and/or realization of a quantum spin Hall insulator in graphene as the nature of the band gap at the Dirac point. Furthermore, we observe the Brillouin-zone-selection effects in photoemission from graphene, similar effects were reported in the literature and were attributed to breaking of the symmetry between A and B sublattices of graphene.

To understand the atomic structure of the intercalated HD-phase of Bi we perform density functional theory (DFT) calculations for various conceivable structural models of the bismuth buffer layer. While most of the symmetry-feasible structures tested in our simulation result in an intact Dirac cone, we have found two which deliver a gap comparable to experiment: i) layer of Bi in (1×1) *on-top* configuration relative to the graphene layer and ii) Bi in form of a two-dimensional (2D) buckled honeycomb lattice – bismuthene. While the first Bi structure has unphysically short interatomic distances, the second is physically allowed as it approaches the dense (111) termination of bulk bismuth. This structure delivers a gap of 60 meV which is of the order of magnitude observed experimentally (190 meV). This finding substantiates the prospect of synthesizing a graphene-bismuthene heterostructure on Ir(111).

II. METHODS

Experiments have been conducted in ultra-high vacuum at a base pressure below 2×10^{-10} mbar. The samples were prepared according to protocols from Ref. [23]. The Ir(111) has been cleaned by repeated cycles of ion (Ar^+) sputtering and annealing at T=1600 K. Graphene was subsequently grown on top by chemical vapour deposition of propene at a partial pressure of 5×10^{-8} mbar with the Ir substrate held at T=1200 K. This procedure results in a high-quality variant of graphene aligned to the Ir lattice (the so called R0° variant), accompanied by the formation of minor domains with rotational displacements close to R30° (rotated relative to the Ir(111) lattice by ∼30°). The low-energy electron diffraction (LEED) pattern of the sample is presented in Fig. 1(a) and does not contain any visible traces of the R30° phase. Proper identification of rotational domains in the course of the study is straightforward both in microscopic studies (by their specific moiré patterns) and in band structure measurements by photoemission [due to the large angular displacement of their surface Brillouin zones (SBZ)]. The R0° rotational variant of graphene shows a characteristic moiré pattern in STM [Fig. 4(a)] arising to 10% lattice mismatch between graphene and Ir(111). This moiré-type lateral modulation of the potential, in turn, gives rise to renowned umklapp-derived band replicas of the Dirac cone (labels "R" in Fig. 2) and minigaps at their crossing points with the primary cone [24–26] (red arrows in Fig. 2).

Many metals can be intercalated under graphene by deposition of the required amount of material on the sample surface (e.g. 1 ML) at room temperature and subsequent annealing (see for example [14, 17, 20, 27]). However, we have observed that for Bi this method is very ineffective and only small amounts of the material can be intercalated in one step, most likely this is due to the low sublimation temperature of Bi (∼ 520 °C) [28]. Intercalation of Bi resulting in the formation of the HD-phase was achieved either by deposition of large amounts of Bi (nominally ∼15 Å as determined from the deposition rate calibrated by a quartz microbalance, assuming Bi density equal to the bulk value of $\rho = 9.8$ g/cm^3) on graphene/Ir(111) held at room temperature and its subsequent annealing at $T = 800$ K for 10 min, or by deposition of Bi on hot graphene/Ir(111) maintained at 720 K for 30 min (deposition rate was 0.6 Å/min in both cases). Sample condition at different stages of preparation was monitored by LEED and XPS (see Figure S1 of the supplemental material). Other methods of preparation were also tested with the aim to reproduce as close as possible the procedures reported by Warmuth et al. in Refs. [22, 29]. This includes deposition on hot substrate (720 K) with either a short post-annealing at 1270 K or short post-annealing at 1370 K with slow cooling to 1020 K (cooling rate < 1 K/s). For all attempted sample preparations we observed ARPES results that are qualitatively the same as those presented in the current paper with only minor differences, therefore the results for those preparations are not shown.

To deposit a "wedge" of Bi thickness the following method was used. During Bi deposition a shutter with a sharp straight edge was moved parallel to the surface of the sample shadowing some part of it from the deposited material. The shutter was translated in discrete steps of constant width at equal time intervals producing a stepped profile of Bi thickness ("wedge").

STM measurements were performed with an Omicron VT STM operated at room temperature. We have used electrochemically etched polycrystalline tungsten tips cleaned as described in Ref. [30].

Band structure mapping of Bi-intercalated graphene has been performed with angle-resolved photoemission using the endstation ARPES 1^2 installed at the beamline UE112-PGM2a at BESSY II. Resolutions of ARPES 1^2 ex-

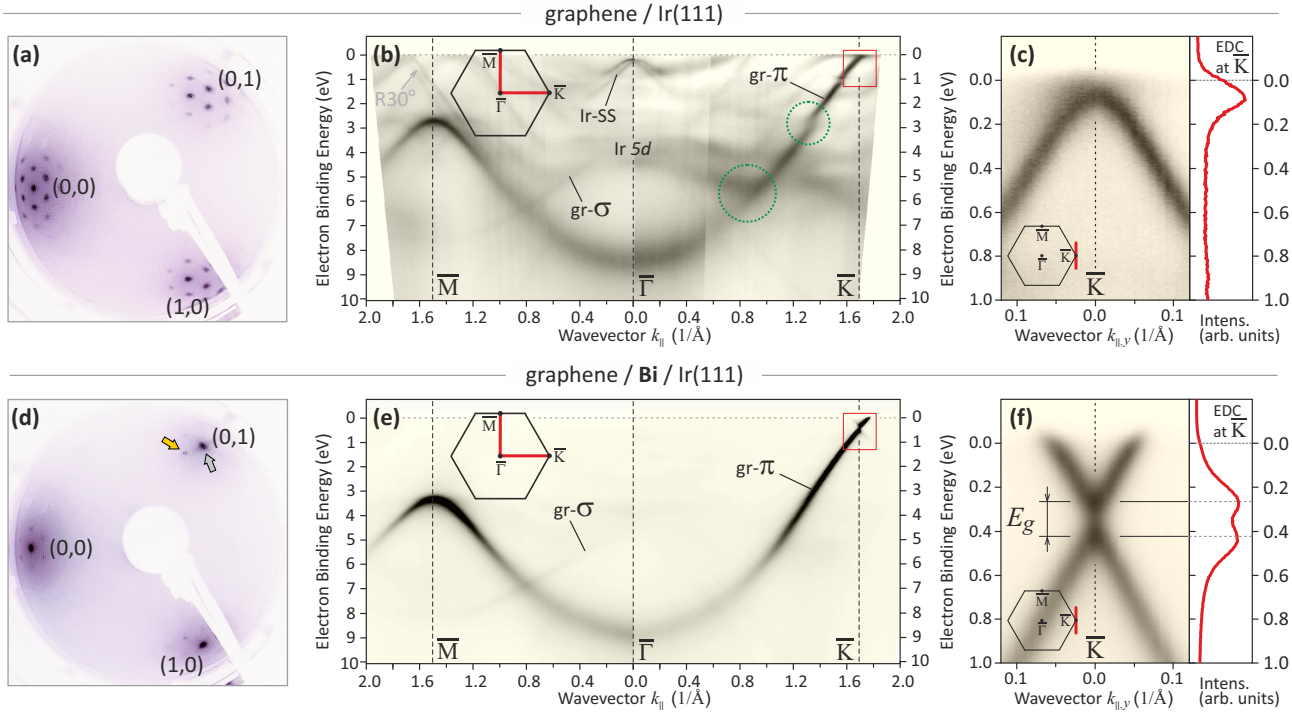

FIG. 1: Identification of HD-phase of Bi-intercalated graphene by low energy electron diffraction (LEED) and angle-resolved photoemission (ARPES); (a-c) Reference data for pristine graphene/Ir(111): (a) LEED with pronounced moiré pattern (beam energy is 53 eV), (b) overall ARPES characterization of band structure along $\overline{\Gamma}-\overline{M}$ and $\overline{\Gamma}-\overline{K}$ directions of the graphene Brillouin zone, (c) high-resolution measurements of Dirac cone at the $\overline{K}$ point. Ir derived features are marked in (b): band gaps due to electronic hybridization between π-band of graphene and *5d* bands of Ir are denoted by green dashed circles, the Ir(111) surface state is labeled as Ir-SS; (d–f) Characterization of Bi-intercalated graphene/Ir(111): (d) LEED pattern with suppressed moiré pattern (beam energy is 53 eV), (e) overall band structure showing quasifreestanding character of graphene and completely suppressed Ir-derived features, (f) Dirac cone revealing n-type of the doping and a relatively small band gap of ∼190 meV.

periment were 0.3° (angular) and 10 meV (energy). The spin-resolved photoemission study was conducted at the endstation/beamline RGBL2 equipped with a hemispherical analyzer Scienta R4000 and 3D spin detector. Angular and energy resolutions of the spin-resolved experiment were 1.5° and 20 meV, respectively. All photoemission measurements have been performed at room temperature. A photon energy of 62 eV and linear polarization of light have been used. The prepared samples have been transferred between ARPES and STM chambers in a vacuum suitcase.

Our studies were complemented by DFT calculations delivering band structure of graphene for various structural configurations of the intercalated bismuth. For structural optimization and band structure calculations the VASP package [31] was used. The projector augmented wave method [32] and the semilocal Perdew-Burke-Ernzerhof [33] approximation to the exchange-correlation energy. The electronic orbitals were expanded using a plane-wave basis with kinetic energies up to 450 eV, a 11×11 Monkhorst-Pack grid was used for the sampling of the basal reciprocal plane [34], and non-local dispersive van der Waals interactions were taken into account with the DFT-D2 method [35]. Supercell band unfolding was performed using the method of Popescu and Zunger [36] implemented in the VaspBandUnfolding code [37] by Qijing Zheng.

III. RESULTS

A. Characterization by LEED and ARPES

The HD phase of Bi-intercalated graphene/Ir(111) can be easily identified by its peculiar structural and electronic properties which are addressed in Figure 1. Most conveniently it can be distinguished by its specific LEED pattern and by band structure mapping in the region of the Dirac cone of graphene using ARPES.

Figs. 1(a–c) serve as a reference and display pristine graphene/Ir(111) before intercalation of Bi. Fig. 1(a) shows its LEED pattern. One sees sharp constellations of spots surrounding primary spots coming from the graphene lattice.

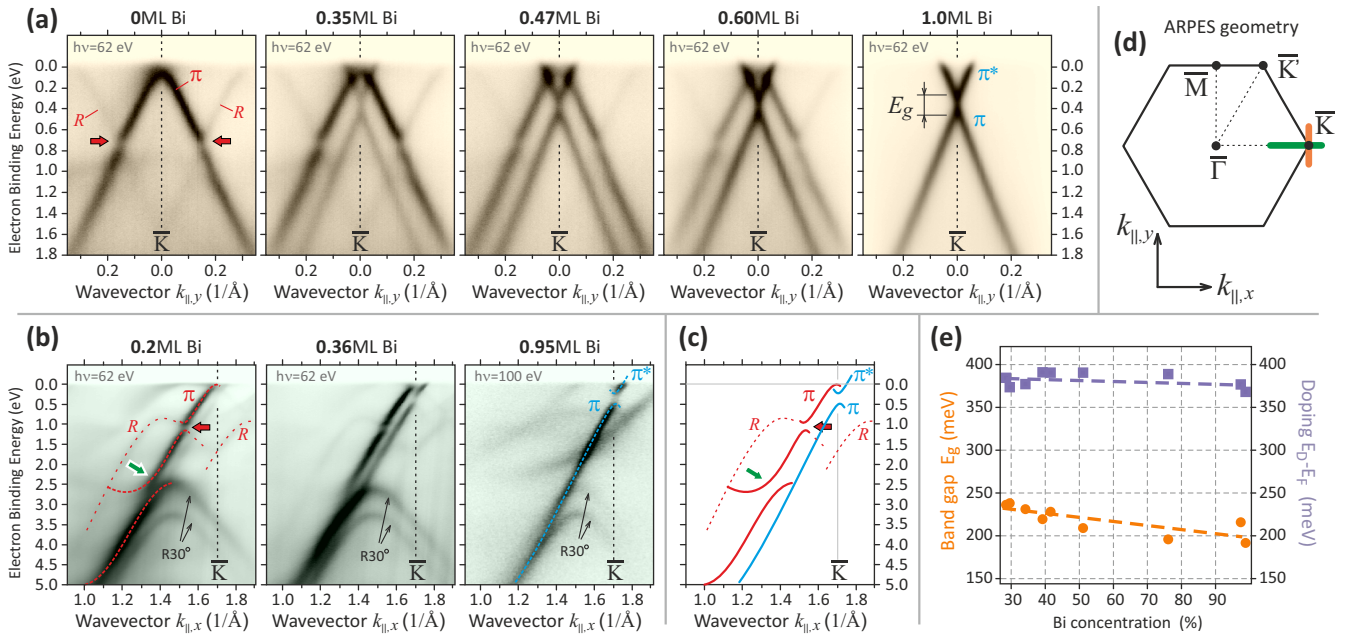

FIG. 2: Behavior of graphene/Ir(111) band structure with increasing concentration of intercalated Bi measured by ARPES; (a) evolution of Dirac cone in graphene measured along the direction perpendicular to $\overline{\Gamma}-\overline{\mathrm{K}}$ line of the surface Brillouin zone (SBZ) [orange line in (d)]. Moiré-induced band replicas are labeled as R, minigaps at the crossing points with main cone are denoted with red arrows; (b) same as (a) but measured along the direction $\overline{\Gamma}-\overline{\mathrm{K}}$ of SBZ [green line in (d)] and at enlarged energy and momentum scale in order to record effect of Bi on band replicas R (red dashed lines) and hybridization gap with Ir (green arrow); (c) band structures of pristine (red) and Bi-intercalated (blue) graphene/Ir(111) extracted from data shown in (b); (d) sketch of experimental geometry of ARPES measurements; (e) extracted behavior of the doping (plot in magenta) and band gap (plot in orange) with increasing concentration of Bi (area covered by intercalated Bi in % of a full layer).

These constellations are related to the moiré pattern occurring due to ∼10% lattice mismatch between graphene and Ir(111) [24, 38]. The moiré beatings are also seen in STM measurements [Figs. 4(a,b)]. They reveal a lateral periodicity of ∼25 Å and z-corrugation of ∼0.3 Å [see trace I in Fig. 4(k)], which is fully consistent with recent surface X-ray diffraction (SXRD) studies [39].

Fig. 1(b) shows the overall band structure of graphene/Ir(111) measured along high-symmetry directions $\overline{\Gamma}-\overline{\mathrm{M}}$ and $\overline{\Gamma}-\overline{\mathrm{K}}$ of the SBZ (see sketch in the inset for experimental geometry). It shows a rich variety of bands from the Ir(111), including Ir *5d* bands at ∼4 eV binding energy and the Rashba-type spin-split Ir(111) surface state [40] (marked as Ir SS) at ∼0.2 eV. The Ir *5d* states hybridize with the π-band of graphene. Hybridization gaps are marked in Fig. 1(b) with green dotted circles. These gaps, which had originally been thought to be due to the graphene superlattice [41], have been addressed in detail in our earlier publication in which we have shown that their origin is electronic hybridization between graphene and Ir [23]. Moreover, it was demonstrated that this hybridization induces a spin-splitting on Dirac fermions in graphene as large as 50 meV [23]. Fig. 1(c) shows the area around $\overline{\mathrm{K}}$ [red rectangle in Fig. 1(b)]. The dispersion was measured perpendicular to $\overline{\Gamma}-\overline{\mathrm{K}}$ (red line in the sketch in the inset). Along this direction photoelectron interference does not cause asymmetry in ARPES intensities of the two sides of the Dirac cone [42, 43]. Graphene is nearly charge neutral, a curvature at the apex of the Dirac cone (just below Fermi level) indicates a band gap of ∼200 meV at Dirac point. In the literature this band gap was assigned to local breaking of the A-B symmetry of graphene sublattices by the Ir(111) substrate [25, 26] accompanied by the coupling of the Dirac cone to Ir bands in the vicinity of $\overline{\mathrm{K}}$ [44]. This band gap at the Dirac point along with strong hybridization with Ir *5d* bands constitutes substantial deviations from the bandstructure of ideal freestanding graphene.

Fig. 1(d–f) display LEED and ARPES characterizations of the HD-phase of Bi-intercalated graphene. As compared to the pristine graphene/Ir [Fig. 1(a)], the moiré-like superstructure of larger periodicity is remarkably suppressed. We observe mainly a superposition of two patterns of primary spots originating from graphene [gray arrow] and from the substrate [yellow arrow] with periodicity similar to that of Ir(111), accompanied by a weak moiré pattern of not higher than first order of diffraction. This indicates the presence of two different lattice constants without significant cross-talk in the diffraction process and reveals loss of coherence between graphene and Ir substrate due to decoupling by Bi. In such situation the Bi buffer layer should *either* have no long-range periodic structure *or* have a surface lattice equivalent to Ir(111) or to graphene, since no third periodicity is observed in the LEED pattern. We also note

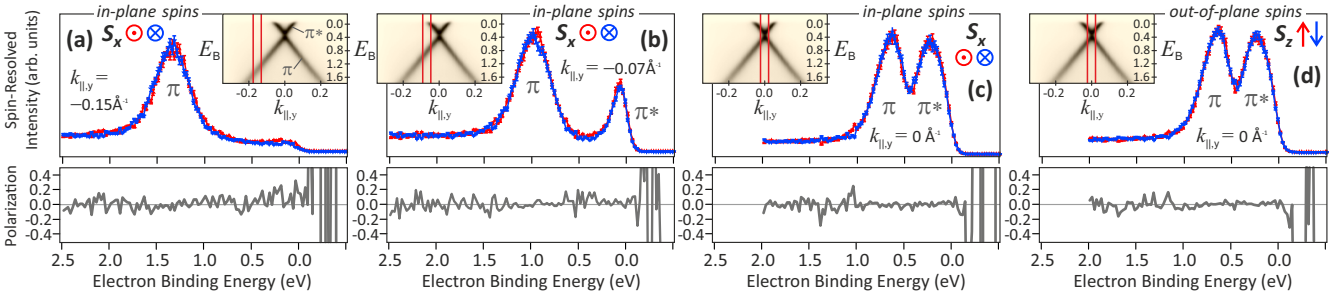

FIG. 3: Probing spin-texture of gapped Dirac cone in Bi-intercalated graphene/Ir(111) by spin- and angle-resolved photoemission. No evidence for a spin-orbit effect is found. (a,b) Rashba-type in-plane component of spin polarization S_x (perpendicular to electron momentum $\mathbf{k}_{\|,y}$) sampled at $\mathbf{k}_{\|,y}$=−0.15 Å^{-1} (a) and $\mathbf{k}_{\|,y}$=−0.07 Å^{-1} (b) relative to $\overline{\mathrm{K}}$ point. Red lines in the insets denote **k**-frames within which spin-resolved energy distribution curves were accumulated. (c,d) In-plane S_x (c) and out-of-plane hedgehog-type S_z (d) spin polarizations of the gap measured precisely at $\overline{\mathrm{K}}$ point. All spin splittings are below detection limit. Dirac cone is spin degenerated, spin texture is absent.

that we do not observe in the diffraction pattern spots rotated relative to graphene by 30°. This excludes, to large extent, the presence in our samples of $(\sqrt{3}\times\sqrt{3})$ $R30°$ superstructure (LD-phase) studied by Warmuth et al. [22]

The band structure of graphene as measured by ARPES reveals significant changes after Bi intercalation [Fig. 1(e)]. Intercalation of Bi suppresses all Ir-derived features visible for pristine graphene/Ir(111) in Fig. 1(b). One sees signals neither from *5d* bands nor from the Ir surface states (Ir SS). Also hybridization [green circles in Fig. 1(b)] between graphene and Ir disappears. Instead, a nearly ideal graphene band structure with only a minor deviation from the freestanding case in the vicinity of the $\overline{\mathrm{K}}$ point [red rectangle, expanded in Fig. 1(f)] is observed. The Dirac cone is nearly perfect, although with n-type doping ($E_\mathrm{D} \sim E_\mathrm{F} - 0.4$ eV) and a relatively small band gap ($E_g \sim 0.19$ eV). The negligible photoemission background seen in Fig. 1(e) indicates a dense and homogeneous Bi layer under the graphene, which prevents photoemission from the buried Ir substrate.

Our aim is to study the origin of the band gap in the Dirac cone of Bi-intercalated graphene and understand whether it is induced by the spin-orbit interactions or arises due to a symmetry distortion of the graphene sublattices. Furthermore, we aim to learn how the gap can be controlled by gradual tuning of the properties of the Bi-graphene interface. Ultimately we aim to approach the solution of the structure of intercalated bismuth in the HD-phase.

B. Dependence on Bi concentration

We have performed a careful study of how the band structure of graphene on Ir(111) changes with increasing concentration of Bi. For that purpose we have intercalated a wedge of Bi with concentrations from 0 to 100%. Here and below we refer to concentration of intercalated Bi, determined from intensity ratios between graphene peaks from intercalated and non-intercalated phases. The absolute amount of Bi deposited on the sample for successful intercalation was ∼5 times higher.

In the presentation of our wedge measurements we mainly concentrate on the Dirac cone in the vicinity of $\overline{\mathrm{K}}$. Its evolution with increasing concentration of Bi is reported in Figure 2. Fig. 2(d) displays a sketch of the experimental geometry. Similarly to the measurements in Figure 1, the Dirac cone at $\overline{\mathrm{K}}$ point has been measured along two directions: perpendicular to $\overline{\Gamma}-\overline{\mathrm{K}}$ [orange line in Fig. 2(d)] and along $\overline{\Gamma}-\overline{\mathrm{K}}$ [green line in Fig. 2(d)]. Series of dispersions acquired for increasing concentration of intercalated Bi in the direction perpendicular to $\overline{\Gamma}-\overline{\mathrm{K}}$ is shown in Fig. 2(a). As mentioned above, in this geometry both sides of the Dirac cone appear equally intense [42, 43]. Fig. 2(b) displays the same dependence but measured along $\overline{\Gamma}-\overline{\mathrm{K}}$ and on larger momentum and energy scales. At this geometry we can capture particularly well, how the electronic hybridization between graphene and Ir evolves with increasing amount of intercalated Bi.

From the ARPES sequences shown in Figure 2 we see that with increasing concentration of Bi the signal of pristine graphene/Ir(111) [first panel in 2(a)] gradually decreases, while a band structure with nearly intact Dirac cone evolves. The Dirac cone of the pristine graphene/Ir shows characteristic features, including charge neutrality, band gap right at the Fermi level (assigned to local *A*-*B* sublattice symmetry breaking [25, 26] accompanied by the coupling of the Dirac cone to Ir bands in the vicinity of $\overline{\mathrm{K}}$ [44]) and moiré-induced band replicas of the main cone (denoted as *R*). The band replicas are accompanied by the occurrence of minigaps at the crossing points with the primary cone [red arrows]. [24, 26] In contrast, the Dirac cone of the HD-phase [last panel in 2(a)] reveals neither band-replicas nor minigaps (similar effect was observed for the LD-phase in Ref. [22]). It exhibits only a small band gap $\mathrm{E}_g \sim 0.19$ eV

and *n*-type doping $E_{\mathrm{D}} \sim E_{\mathrm{F}} - 0.4$ eV. This perfectly demonstrates decoupling of graphene from Ir(111) by Bi and its nearly quasifreestanding character. Due to *n*-doping both π (bonding) and π^* (antibonding) cones are seen below the Fermi level and the band gap and energy shift of the Dirac point can be determined very precisely.

For intermediate concentrations of Bi we observe a superposition of signals from the pristine graphene/Ir(111) and from the fully intercalated graphene. This means that intercalation takes place in a *lateral phase segregation* regime: Bi under graphene forms islands separated by non-intercalated areas of pristine graphene/Ir(111). In such scenario the band structures of both types of the sample surface are summed up and captured simultaneously due to the large size of the photon beam in the ARPES experiment ($\sim 20 \times 400\ \mu m^2$) which exceeds dimensions of intercalated and non-intercalated areas by far (typically several 100 of nm, according to our STM measurements).

From the data shown in Fig. 2(a) we have extracted the band gap at the Dirac point along with charge doping for various concentrations of Bi. The results are summarized in Fig. 2(e). While the doping does not change with Bi concentration [$E_{\mathrm{D}} = E_{\mathrm{F}} - 380$ ($\pm$5) meV] the band gap E_g decreases with increasing amount of Bi from $E_g = 240$ ($\pm$5) meV to $E_g = 185$ ($\pm$5) meV. Considering Bi intercalation in the phase segregation regime, this effect is surprising since it shows that along with an increasing amount of Bi not only the intercalated Bi islands laterally enlarge, but also there can be small structural variations within Bi islands depending on their size, apparently affecting the graphene lattice and the magnitude of the band gap.

ARPES data reported in Fig. 2(b) show the Dirac cone in the HD-phase for increasing Bi concentration, but measured along the direction $\overline{\Gamma} - \overline{\mathrm{K}}$ of the SBZ [denoted with green line in Fig. 2(d)]. Note that in this experimental geometry only one side of the Dirac cone is seen due to the Brillouin-zone-selection effect [42, 43]. Dispersions are shown on enlarged scale in which also hybridization gaps with *5d* bands of Ir are observable [green arrow in Fig. 2(b)]. We have to note that there is a minor contribution from a R30° rotation variant [denoted in Fig. 2(b)] in a particular sample but it is irrelevant for our analysis. Consistently with data in Fig. 2(a) we see that with the increasing amount of intercalated Bi not only replicas of the π-band (R) and related to them minigaps (red arrows) disappear, but also band gaps caused by hybridization with Ir vanish. This further confirms that Bi decouples graphene from the Ir(111) substrate. The extracted band structures of pristine graphene/Ir(111) and of the HD-phase along the direction $\overline{\Gamma} - \overline{\mathrm{K}}$ of the SBZ are superimposed in Fig. 2(c) by red and blue lines, respectively.

C. Probing the spin texture of the Dirac cone

An important key to the nature of the band gap at Dirac point of Bi-intercalated graphene is its spin-texture, which can be measured by spin-resolved photoemission. In a recent study on Pb-intercalated graphene/Pt(111), Klimovskikh et al. [20] reported a Dirac cone gapped due to spin-orbit interaction induced in graphene by the underlying Pb layer. Klimovskikh et al. argue that heavy *sp*-metals such as Pb avoid the predominant Rashba effect induced by hybridization with d states as in Au [7, 19]. Away from the Dirac cone, the spin splitting was found to be smaller than 10 meV setting the limit for an induced Rashba-type spin-orbit interaction. In addition, a spin-orbit interaction can be induced that is equivalent to an intrinsic spin-orbit interaction. The observation of an in-plane spin polarization at the upper edge of the $\sim$ 200 meV wide gap is seen as indication that the induced intrinsic spin-orbit interaction is larger than the one of Rashba type [20]. Sublattice asymmetry was found to be absent based on qualitative photoemission intensity arguments. Therefore, it was concluded [20] that the system fulfills the preconditions for realization of the quantum spin Hall effect [45].

In order to test whether we encounter same scenario in the present case of graphene intercalated with the HD-phase of Bi, we investigated the spin texture of the Dirac cone using spin- and angle-resolved photoemission. Key results are shown in Figure 3 (more details are provided in Figure S2 of supplementary material). We have probed 3D spin components at several momentum vectors $\mathbf{k}_{\parallel}$ precisely at and around the $\overline{\mathrm{K}}$ point of graphene.

Figs. 3(a,b) display spin polarization S_x and corresponding energy distribution curves (EDC) measured off the $\overline{\mathrm{K}}$ point in the direction of $\mathbf{k}_{\parallel,y}$ which is perpendicular to $\overline{\Gamma} - \overline{\mathrm{K}}$. The spin polarization S_x is in plane and perpendicular to the wavevector $\mathbf{k}_{\parallel,y}$, i.e., the direction that should reveal a Rashba-type spin polarization of the Dirac cone, if present. Fig. 3(a) displays a measurement at $\mathbf{k}_{\parallel,y}$=-0.15 Å^{-1} (referred to $\overline{\mathrm{K}}$) and probes the in-plane spin polarization of the lower Dirac cone (valence band π) somewhat away from $\overline{\mathrm{K}}$. Since a spin-orbit gap induced by intrinsic spin-orbit interaction leads to different magnitudes of the spin splitting in lower (π) and upper (π^*) Dirac cone [20], we test the spin polarization within both π and π^* bands. This is possible because graphene/Bi/Ir(111) is *n*-doped and the conduction band π^* can be accessed by photoemission. Spin-resolved EDC simultaneously probing π and π^* closer to $\overline{\mathrm{K}}$, i.e., at $\mathbf{k}_{\parallel,y}$=-0.07 Å^{-1}, is shown in Fig. 3(b). Neither the spectra in Fig. 3(a) nor those in Fig. 3(b) show any detectable spin polarization hence evidencing the absence of a Rashba-type spin-orbit effect. This result is generally in line [13] with the absence of electronic hybridization between graphene and Bi evidenced by ARPES in Fig. 1(e).

We proceed further with looking at the spin-texture of the gap at the Dirac point at $\overline{\mathrm{K}}$. Figs. 3(c) and 3(d) display in-plane S_x and out-of-plane S_z spin components. Also in this case we do not observe a detectable spin polarization

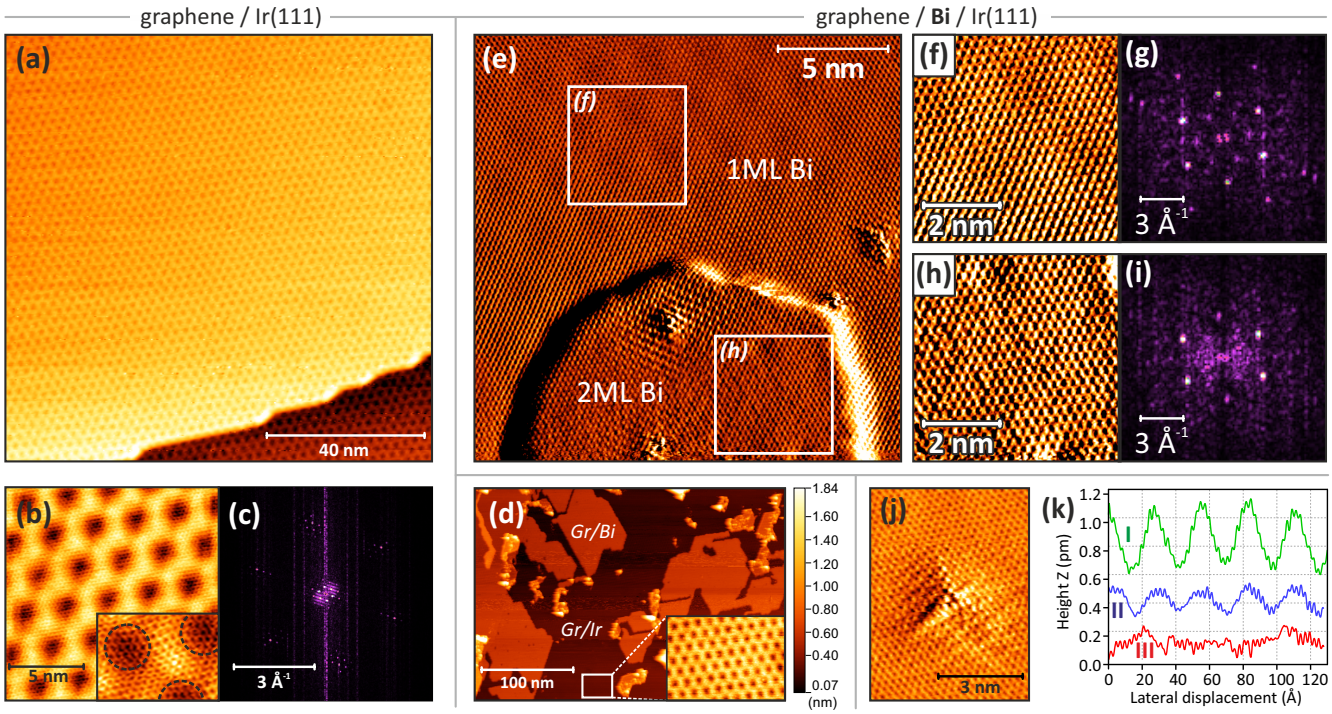

FIG. 4: STM characterization of pure (a-c) and Bi-intercalated (d-k) graphene on Ir(111). (a) Large scale STM image of graphene/Ir(111) showing a moiré pattern. Graphene covers a step edge like a carpet. (b) Close up of the moiré pattern from (a), the inset displays a graphene honeycomb lattice (current channel). See also Figure S7 in supplemental material. (c) Fourier transform (FT) of (b). (d) Graphene/Ir(111) partially intercalated with Bi reveals islands of Bi with straight edges and the typical moiré pattern of graphene/Ir(111) in areas between the islands (a close up of such area is displayed in the inset). (e-i) STM characterization of fully intercalated graphene/Bi/Ir(111) sample (current channel). In (e) one can observe simultaneously areas with 1 (top) and 2 (island at the bottom) monolayers (ML) of intercalated Bi. Zoom in these areas is presented in (f) and (h), respectively, and corresponding FT images are shown in (g) and (i). For both areas one can see standing waves of electron density that can be detected by STM, these standing waves are formed by electrons scattering at small defects. A close up of such standing wave pattern is presented in (j), where scattering occurs at a point defect in the center. Panel (k) compares topographic line profiles traced along the [01] direction for (I) graphene/Ir(111), (II) graphene/1 ML Bi/Ir(111), (III) graphene/2 ML Bi/Ir(111). Profiles are arbitrarily displaced along the vertical axis for better visualization. Tunneling parameters are: (a,b) 2 mV/0.5 nA; (d) 0.8 V/0.45 nA; (e,f,h) 0.24 V/2.1 nA; (j) 2 mV/0.67 nA.

neither in plane nor out of plane. This excludes the presence of enhanced intrinsic spin-orbit interaction as reported for the case of graphene on Pb by Klimovskikh et al. [20].

We want to emphasize that our results also exclude a hedgehog-like out-of-plane reorientation of spins in the gap [18, 19], as seen from zero in-gap spin polarization S_z shown in Fig. 3(d). An out-of-plane spin polarization of the gap can result when the sublattice asymmetry of graphene is broken and a Rashba effect is present. Since one of the two conditions, the Rashba effect, is not met, as one sees from zero in-plane spin polarizations S_x [Figs. 3(a) and 3(b)], the results in Fig. 3 are consistent.

To conclude, the fully spin degenerate Dirac cone does not give any indication for a spin-orbit origin of the gap at the Dirac point. That motivates to search for its origin in structural properties of the graphene-Bi interface, and we proceed with a microscopic study.

D. Structural study with STM

We show characterization by STM in Figure 4. STM measurements of pristine graphene/Ir(111) are displayed in Figs. 4(a–c) for reference. In the large scale image in Fig. 4(a) one sees a periodic beating of moiré with lateral periodicity of ∼25Å and weak z-corrugation of ∼0.3Å [see topographic trace I in Fig. 4(k)]. The measured magnitude of z-corrugation is of structural (and not electronic) origin as it was confirmed by SXRD experiments [39]. Fig. 4(b) and its zoom in the inset show an atomically resolved image of graphene/Ir(111) in which the local breaking of A-B symmetry is observable: areas showing non-equivalent signal from graphene sublattices [23] are emphasized in the

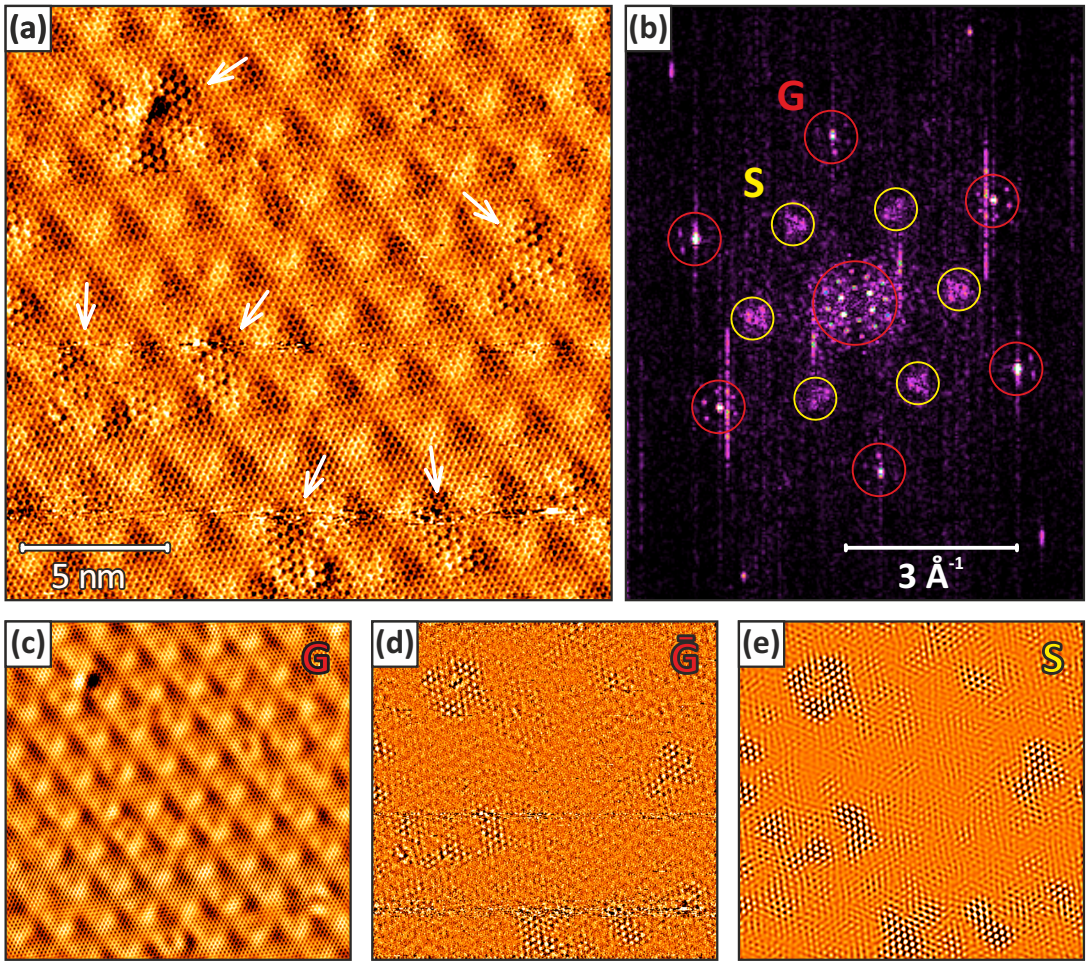

FIG. 5: Local observation of fragmented "hauberk"-like pattern of low-density Bi phase $(\sqrt{3} \times \sqrt{3})$ $R30°$ in graphene/1 ML Bi/Ir(111). (a) Raw STM image (current channel) shows areas on the surface with locally different appearance ($U_t = 2$ mV, $I_t = 1.6$ nA). "Hauberk" textures are marked with white arrows. Fourier transform (FT) of (a) presented in figure (b) reveals two different periodic patterns with hexagonal symmetry: a bright one coming from the graphene lattice with superstructural spots of moiré (areas marked with red circles, G) and a $(\sqrt{3} \times \sqrt{3})$ $R30°$ periodic lattice (areas marked with yellow circles, S). To show where S periodicity appears in the real-space image (a) we apply FT filtering and display filtered images corresponding to only G pattern (c), everything except G pattern ($\overline{\text{G}}$) (d) and only S pattern of $(\sqrt{3} \times \sqrt{3})$ $R30°$ superstructure (e).

inset by dashed circles (larger scale atomically resolved image is available in supplemental material as Figure S7). Such local symmetry breaking was earlier proposed as the origin of the band gap in pristine graphene/Ir(111) [26]. Fig. 4(c) shows a Fourier transform of the larger scale STM image from Fig. 4(b) in which peaks with hexagonal arrangement related to the moiré pattern are seen.

The STM images change drastically upon intercalation of Bi and formation of the HD-phase. The results are shown in Figs. 4(e–j). Fig. 4(d) displays the image of a sub-monolayer (nominally 0.3 ML) amount of intercalated Bi. One sees that the intercalation occurs in the phase segregation regime: Bi initially forms 1 ML-thick islands at the interface while some areas remain free of Bi. Intercalated islands of Bi can be identified by the nearly absent moiré pattern which, in contrast, is clearly seen in the surrounding areas of pristine graphene/Ir(111). These observations are fully consistent with ARPES data taken for gradual intercalation of Bi [Figs. 2(a) and 2(b)] which also support the phase segregation type of intercalation.

As compared to the results of the STM characterization of the LD-phase by Warmuth et al. [22], our STM images of the HD-phase reveal a strikingly different morphology of Bi buffer layer. On the major area of the sample surface we neither observe the $(\sqrt{3} \times \sqrt{3})$ $R30°$ structure [rotated by 30° relative to Ir(111) and with a factor of $\sqrt{3}$ larger periodicity] nor the meandering dislocation pattern composed of double lines [22]. Instead, we see a smooth surface with very weak periodic beatings resembling the original moiré pattern of graphene/Ir(111).

Fig. 4(e) shows results of intercalation with a higher amount of Bi (nominally 0.9 ML). For the area shown, one sees

that the intercalation is complete since the pronounced moiré pattern characteristic of graphene/Ir(111) is not seen anywhere. In addition, we systematically see in our data that formation of a second (and even third) Bi monolayer under graphene takes place. The area hosting 2 ML Bi under graphene is denoted in Fig. 4(e). We take a closer look at graphene above 1 ML and 2 ML of Bi. Atomically resolved images of corresponding areas from Fig. 4(e) are displayed in Figs. 4(f) (1 ML) and 4(h) (2 ML). In both cases we do not see a strong dominance of one sublattice over the other. This qualitatively indicates a rather weak *A*-*B* sublattice asymmetry not contradicting the moderate band gap observed in the Dirac cone by ARPES [Fig. 1(f)]. On the atomic scale we cannot distinguish the two phases, however intercalation of a second monolayer of Bi is strongly supported by differences in the moiré pattern. Indeed, the moiré above Bi is extremely weak but very well periodic as confirmed by a Fourier transform (FT) analysis [Fig. 5(b), not resolved in Fig. 4(g) due to the small size of the original image]. The FT map shows well-defined frequencies corresponding to the moiré period, and they are the same as for pristine graphene/Ir(111) [Fig. 4(c)]. A topographic profile of the moiré of the HD-phase of Bi-intercalated graphene compared to that of graphene/Ir(111) is shown in Fig. 4(k) [see trace II] and reveals the lateral periodicity of ∼25 Å and a *z*-corrugation of ∼0.1 Å. If we look at the data measured from above a 2 ML-thick Bi island [STM image in Fig. 4(h), its FT map in Fig. 4(i) and its featureless topographic trace III in Fig. 4(k)], we see that even this weak moiré pattern is absent when graphene is hosted above 2 ML of Bi. This suggests complete decoupling of graphene from Ir by intercalated Bi at thicknesses above 1 ML.

We identify the weak moiré seen over areas with 1 ML of intercalated Bi as purely electronic effect possibly arising from electronic interference with Ir(111) through the Bi interlayer. Indirect evidence for this is obtained from the STM imaging of structural defects of graphene (or its substrate), an example of which is shown in Fig. 4(j). The star-like distortions are seen in the surroundings of the defect. These distortions have been ascribed in the literature to the scattering of graphene electrons on point defects and to the formation of standing waves [46]. Analysis of STM data (both topographic channel and channel of tunneling current) reveals that the amplitude of the tunneling signal arising from the standing waves is larger than the amplitude of *z*-corrugation from the moiré pattern of graphene intercalated with 1 ML of Bi [see trace III in Fig. 4(k)] This, in turn, suggests that the weak moiré could also be an electronic effect. Such conclusion would also be consistent (i) with LEED data in Fig. 1(e) which shows for the HD-phase very low-intensity superstructural reflexes characteristic of the moiré pattern and (ii) with the ARPES characterization of the band structure revealing no *umklapp* band replicas of the Dirac cone [Figure 2], which are known to be present even in the systems with poor lateral coherence [19].

Another proof that the HD-phase reported in the present work contains a higher concentration of Bi as compared to the LD-phase reported by Warmuth et al. [22] is delivered by the observation of local traces of the LD-phase in our samples. Fig. 5(a) shows an exemplary STM image of Bi-intercalated graphene which, apart from a weak moiré periodicity, shows several spots with remarkable "hauberk"-like texture (marked with white arrows in the figure). Such textures can be found locally at different sites of the sample but they cover a very minor part of the surface area. Analysis of the FT power spectrum is shown in Fig. 5(b). It reveals two sets of structural spots which are marked as G (red) and S (yellow) and denote periodicities associated with graphene (with weak moiré pattern) and a $(\sqrt{3} \times \sqrt{3})$ $R30°$ superstructure, respectively. In order to separate and visualize contributions of these two, we have performed FT filtering. Results are shown in Figs. 5(c–e). Figure 5(c) displays an image corresponding to the G pattern and represents the unperturbed moiré-type graphene carpet. The "hauberk" becomes visible in Fig. 5(d) which displays filtering by all FT frequencies except for the G pattern ($\overline{\mathrm{G}}$). It is, however, revealed in the most detailed manner in Fig. 5(e) which shows filtered data corresponding to S pattern frequencies only. Comparing these results to Ref. [22] we realize that the observed "hauberk" texture has the same $(\sqrt{3} \times \sqrt{3})$ $R30°$ pattern as the LD-phase reported by Warmuth et al. [22], however excluding the double-line dislocation network. In our samples the "hauberk" texture emerges locally and non-systematically, which could also be related to reduced local concentration of Bi in the corresponding areas. Altogether we assume that the "hauberk" texture may be associated with the LD-phase.

IV. DISCUSSION

A. Origin of the band gap

We have observed that intercalation of graphene/Ir(111) with Bi decouples graphene from the Ir substrate and largely restores the bandstructure of quasifreestanding graphene, which shows neither band replicas, nor hybridization effects with Ir *5d* bands. The only deviations from ideal graphene are *n*-type doping and a band gap at the Dirac point the size of which depends on the Bi concentration [Fig. 2(e)]. The most interesting question is the origin of the band gap and the reasons for its tunability. Since the measurements with spin-resolved photoemission do not give any indication of a spin-orbit origin of the gap, we concentrate on structural properties.

First of all, we will consider corrugation as a possible origin. Warmuth et al. [22] have proposed a disturbed

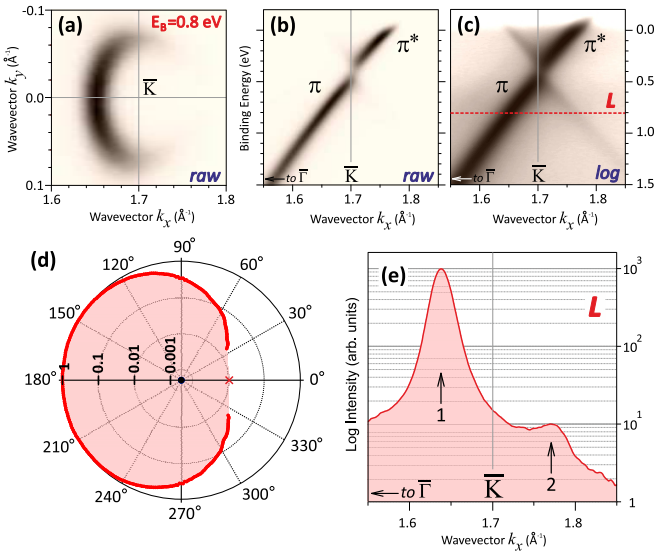

FIG. 6: Brillouin-zone-selection effects in Bi-intercalated graphene. (a) Constant energy surface of Dirac cone sliced at the binding energy of ∼0.8 eV reveals strongly anisotropic intensity distribution around the $\overline{\mathrm{K}}$ point of the SBZ; (b,c) dispersion of the Dirac cone measured along the $\overline{\Gamma}-\overline{\mathrm{K}}$ line of the SBZ, precise alignment angles were determined from complete photoemission mapping. Raw data (b) and intensity plot in logarithmic scale (c) are shown; (d) Polar plot shows normalized photoemission intensity of the Dirac cone as a function of azimuthal orientation of the trace passing through the $\overline{\mathrm{K}}$ point; (e) momentum distribution curve (MDC) at 0.9 eV binding energy extracted from (c) reveals relation between the intensities of Dirac cone in 1^{st} (arrow 1) and 2^{nd} (arrow 2) SBZ. Position of the slice is denoted in (c) with red dashed line.

graphene lattice and modulated distance between graphene and Ir atoms as the reason for the gap. Due to this and in a view of the presently observed, although extremely weak, moiré pattern in the HD-phase we have tested the effect of z-corrugation (Δz) on the band gap using density functional theory (DFT). Our model of corrugated graphene without substrate accounts exclusively for geometric parameters. The model reflects the real lateral moiré periodicity ($\sim$ 25 Å) and, hence, was built as (10×10) graphene supercell with artificially induced corrugation of ∼1 Å, which exceeds by far not only the small corrugation in Bi-intercalated graphene, but also the original corrugation in pristine graphene/Ir(111) ($\Delta z \sim 0.3$ Å) [Fig. 4(k)]. The obtained E_g (not shown) was only a few meV, which is incomparably smaller than the value measured by ARPES ($E_g \sim 190$ meV) [Fig. 2]. This means that the moiré-type corrugation observed in our HD-phase of graphene cannot be the physical reason for the band gap in the Dirac cone.

Hybridization of graphene states with d-states which was proposed as explanation of the band gap in Cu-intercalated graphene on Ir(111) [27] can be excluded in our case, since Bi has no d-states in the valence band and the π-band of graphene shows no hybridization with Bi states [Fig. 1(e)].

Based on our STM data [Figs. 4 and 5] which shows graphene with homogeneous honeycomb cells and, hence, reveals large degree of equivalence of all carbon atoms within each hexagon, we can also exclude local rehybridization of graphene (from sp^2 to sp^3) [47] as origin of the band gap. Such rehybridization would lead to the formation of an accordeon-like texture of graphene with extreme nonequivalence of the A and B sublattices which would be clearly seen in STM. Furthermore, such effects are responsible for gaps that are much larger than the one observed in the present case. For instance, in hydrogenated graphene on Ir(111), the gap E_g exceeds 1 eV [48].

The analytical model most commonly used to explain the relatively small band gaps at the Dirac point is a weak breaking of the A-B symmetry of graphene sublattices due to a difference (Δ) in the electrostatic on-site potentials [43, 49–51]. In the case of non-zero difference Δ, the band dispersion of the Dirac cone acquires in the vicinity of the Dirac energy a parabolic character and a band gap of magnitude Δ opens at the Dirac point.

It has already been mentioned that the honeycomb structure of graphene gives rise to so called Brillouin-zone-selection effects in the angular distribution of photoemission intensity within the Dirac cone [42, 43]. In particular, constructive/destructive interference results in a strongly anisotropic intensity distribution around the $\overline{\mathrm{K}}$ point. This is seen in Fig. 6(a) which shows a constant energy surface of the HD-phase sliced at a binding energy ∼0.8 eV somewhat below the Dirac point. One sees a pronounced intensity within the 1^{st} SBZ with absolute maximum at the $\overline{\Gamma}-\overline{\mathrm{K}}$ line, and suppressed intensity in the 2^{nd} SBZ with absolute minimum also along $\overline{\Gamma}-\overline{\mathrm{K}}$, forming the so called "dark corridor" of intensity [52]. This is the situation for the π states, but it mirror-reverses for π^* states.

Breaking of A-B sublattice symmetry not only opens a gap at the Dirac point but also disturbs the phase cancellation that affects the photoelectron intensity from the Dirac cone. In this way, Bostwick et al. [43] have adopted the

formalism of Shirley et al. [42] and showed that the relation between photoelectron intensities from opposite sides of the Dirac cone measured precisely at the $\overline{\Gamma}-\overline{\mathrm{K}}$ line in 1^{st} and 2^{nd} SBZ correlates with the width of the band gap at the Dirac point and can, in principle, serve as a measure for it.

Such approach is not fully universal, since in a realistic model even for freestanding graphene, the photoelectron intensity in the "dark corridor" is not exactly zero and depends on the experimental conditions, such as light polarization and photon energy [52]. However, it can be used quite efficiently when the preconditions outlined by Gierz et al. [52] are met. In particular, use of *p*-polarized light and higher photon energies ($h\nu > 60$ eV) where illumination of the "dark corridor" is significantly reduced [52], do enable the application of the model suggested by Bostwick et al. [43] for estimation of an upper limit for the degree of sublattice symmetry breaking.

We have done this type of analysis, and the results are reported in Figure 6. For achieving precise alignment and cut of the Dirac cone through the $\overline{\mathrm{K}}$ point and along the $\overline{\Gamma}-\overline{\mathrm{K}}$ direction, we have conducted a complete photoemission mapping of the Dirac cone $I(E, \mathbf{k}_{\parallel,x}, \mathbf{k}_{\parallel,y})$ with high momentum resolution. An example of an acquired constant energy surface is seen in Fig. 6(a). A dispersion measured along $\overline{\Gamma}-\overline{\mathrm{K}}$ is shown in Figs. 6(b,c), a momentum distribution curve (MDC) at the binding energy of 0.8 eV [denoted by a red dashed line in Fig. 6(c)] is plotted in Fig. 6(e). The overall behavior of the photoemission intensity of the Dirac cone traced for different azimuthal directions passing through the $\overline{\mathrm{K}}$ point is plotted in Fig. 6(d). The value for the 0° azimuth (marked with a cross) was extracted from a separate high-statistics spectrum acquired in the same geometry [Figs. 6(b,c)]. From Figs. 6(d,e) one sees that the ratio of intensities of graphene peaks along the $\overline{\Gamma}-\overline{\mathrm{K}}$ line in 1^{st} and 2^{nd} SBZ is as small as 1/100. According to the criteria suggested by Bostwick et al. [43] this value corresponds to a gap of around 140 meV in the *A*-*B* symmetry breaking model, which is well consistent with the experimental gap value of ∼190 meV. Hence we conclude on *A*-*B* sublattice symmetry breaking as a plausible explanation of the observed band gap $\mathrm{E}_g \sim 190$ meV in the HD-phase of Bi-intercalated graphene under the conditions of this model. However, an unambiguous proof will require experimental information about the atomic structure of intercalated Bi.

Such mechanism would also help to explain the reduction of the band gap with increasing Bi concentration in the intercalated interlayer [Fig. 2(e)]. Indeed, in the case of Bi atomic structure that promotes a sublattice asymmetry in graphene this effect can be related to stronger *A*-*B* asymmetry above small Bi islands which can grow in registry with the substrate, while in larger islands this asymmetry will be reduced due to lattice mismatch.

We need to mention here that there is also a purely instrumental factor that influences the size of the apparent gap in ARPES. Some minor overestimation of the gap value is always present in the experiment due to finite momentum resolution in the direction perpendicular to the plane of the measured dispersion. This resolution is determined by the size of the electron analyzer entrance slit and results in averaging of the spectrum over a range of momenta, which effectively increases the apparent curvature of the cone apex. This effect is very important to take into account for bands with steep dispersion, such as the Dirac cone of graphene. For our close-up ARPES measurements a 0.35° analyzer slit was used and we estimate that it can be responsible for up to $\sim 30-40$ meV apparent increase of the E_g value (see Figure S5 of supplemental material).

Another physical mechanism that can lead to an apparent gap in the ARPES of the Dirac cone is electron-plasmon coupling. This effect was observed for graphene on dielectric substrates [53] and it manifests itself in ARPES as two apparent Dirac cones shifted in energy. This effect may be of importance if intercalated Bi forms a bismuthene structure discussed in the next section, since freestanding bismuthene is predicted to be a narrow-gap semiconductor. Moreover, in our data we indeed observe a relatively small shift in energy between the linear parts of upper and lower cones (see e.g. Fig. 1(f) and Fig. S6(a) in the supplemental material). However, we cannot directly attribute this shift to electron-plasmon coupling effects because a similar shift can appear in the experimental data due to instrumental reasons mentioned above, namely the finite width of the analyzer slit (see Fig. S6 for details).

B. Consideration of the atomic structure

In order to approach a solution of the atomic structure of the intercalated Bi, we have performed an extensive DFT study aiming to find among the various possible structures those that would reproduce the magnitude of the band gap at Dirac point (E_g) seen in the ARPES experiment.

First we have considered (2×2) and $(\sqrt{3}\times\sqrt{3})$ *R*30° Bi superstructures that form a dense monolayer of Bi atoms under graphene. Even though these structures do not fully corroborate our LEED [Fig. 1] and STM [Fig. 4] results, as no corresponding superstructural periodicities are seen in the LEED and STM data (except for minor non-systematic traces of $(\sqrt{3}\times\sqrt{3})$ *R*30° in Fig. 5) they can serve as good approximation for testing the effect of bismuth on the sublattice asymmetry in graphene.

In the course of simulation these structures were placed relative to graphene in either *on-top* configuration, in which intercalated Bi atoms are directly below the carbon atoms, or *hollow-site* configuration, in which Bi atoms are residing below the centers of graphene hexagons. The obtained band structures of $(\sqrt{3}\times\sqrt{3})$ *R*30° and (2×2) for

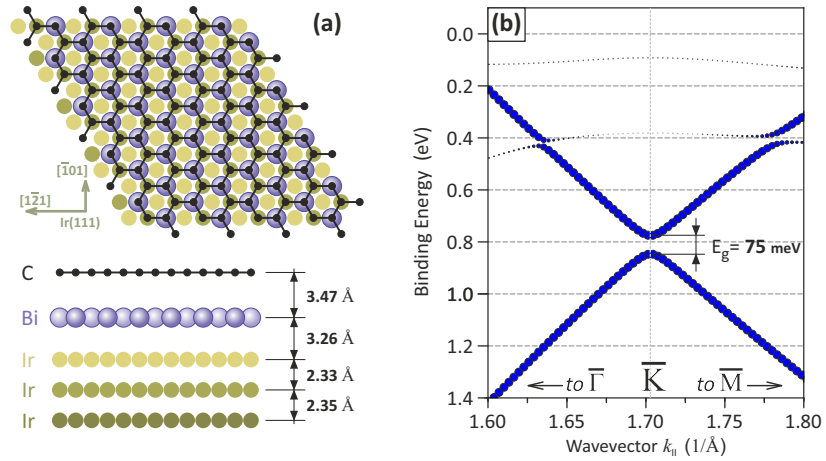

FIG. 7: Density functional theory study of (1×1) Bi-intercalated graphene on Ir(111). *On-top* graphene/Bi configuration. (a) Structural model of graphene/Bi/Ir(111) shown as top view (upper panel) and side view (lower panel, view direction is along Ir[1$\bar{2}$1]). (b) Band structure of graphene/Bi/Ir(111) near $\overline{\text{K}}$ traced along $\overline{\Gamma} - \overline{\text{K}} - \overline{\text{M}}$. Band gap at the Dirac point is $E_g \sim 75$ meV.

the hollow-site configuration are shown in Fig. S3 of supplemental material. Interestingly, although Bi *sp*-bands form hybridization gaps with the graphene Dirac cone, *no band gap* occurs precisely at the Dirac point (the same is true for the *on-top* configuration). This result is in line with calculations of Warmuth et al. [22], where absence of the band gap in graphene/Bi/Ir(111) was predicted for a variety of Bi structures of different density in a $(\sqrt{3}\times\sqrt{3})$ $R30°$ supercell.

To explore a case of extreme sublattice symmetry breaking we tested (1×1) graphene/Bi. We emphasize that such system is hypothetical because distances between Bi atoms are shorter than twice their covalent radius. For (1×1) one can achieve strongest symmetry breaking when artificially placing carbon atoms from one graphene sublattice right above atoms of Bi in the *on-top* configuration [Figure S4(a) of supplemental material]. In such case a band gap of $E_g \sim 100$ meV is indeed predicted. Its magnitude, however, is still smaller than experimentally observed value $E_g \sim 190$ meV. This remarkable result shows that *the overall interaction between graphene and Bi is weak*. This can be ascribed to a weak (if any) electronic hybridization between them. When the (1×1) case is considered in the more symmetric *hollow-site* configuration (Bi atoms reside at the centers of graphene hexagons) the band gap vanishes completely [Figure S4(b) of supplemental material]. We have conducted a more detailed study including the Ir(111) substrate, the results for the *on-top* configuration are presented in Figure 7. The band gap at the Dirac point is $E_g \sim 75$ meV, which is reduced compared to the results without the substrate. The doping value $E_D \sim 0.8$ eV is significantly larger than the experimental one.

We have also considered several structures commensurate with longer period to take into account a possible moiré pattern [results not shown]. In this case the doping value $E_D \sim 0.5$ eV was close to the one experimentally observed, however the size of the band gap was not reproduced in the studied structures. We also tested energetically unfavorable [22] alloyed phases acquired by substituting Ir atoms from first atomic layer of Ir substrate with atoms of Bi according to either (2×2) or $(\sqrt{3}\times\sqrt{3})$ $R30°$ patterns. The band structures [not shown] were rather similar to those of non-alloyed intercalated Bi superstructures (2×2) and $(\sqrt{3}\times\sqrt{3})$ $R30°$ and did not reveal a gap at the Dirac point of graphene.

It is truly remarkable that the only physically realistic structure (among tested conceivable models) delivering a gapped Dirac cone with E_g somewhat comparable to that seen in experiment, was a layer of bismuthene placed between graphene and Ir(111), even though it does not directly provide a sublattice symmetry breaking in graphene. The corresponding relaxed structural model is shown in Figure 8(a) as top and side views. Bismuthene is a buckled honeycomb network of Bi atoms with sublattices A and B displaced relative to each other by 1.81 Å in z direction. Bismuthene is also an elementary structural block of (111) termination of bulk Bi [54] and hence the densest structure suitable to approximate the HD-phase of intercalated Bi. A systematic classification of commensurate graphene-bismuthene heterostructures was proposed by Naumov and Dev [54]. The unit cell of bismuthene is larger than that of graphene and in our model it forms a $(\sqrt{3}\times\sqrt{3})$ $R30°$ hexagonal superstructure commensurate with graphene with a minor compression of the lattice constant by 2%. Such a remarkable coincidence means that if a commensurate graphene-bismuthene structure is realized in practice, a moiré pattern due to lattice mismatch will be formed not at the graphene/Bi, but at the Bi/Ir interface and will have a period similar to the moiré of graphene/Ir(111), in agreement

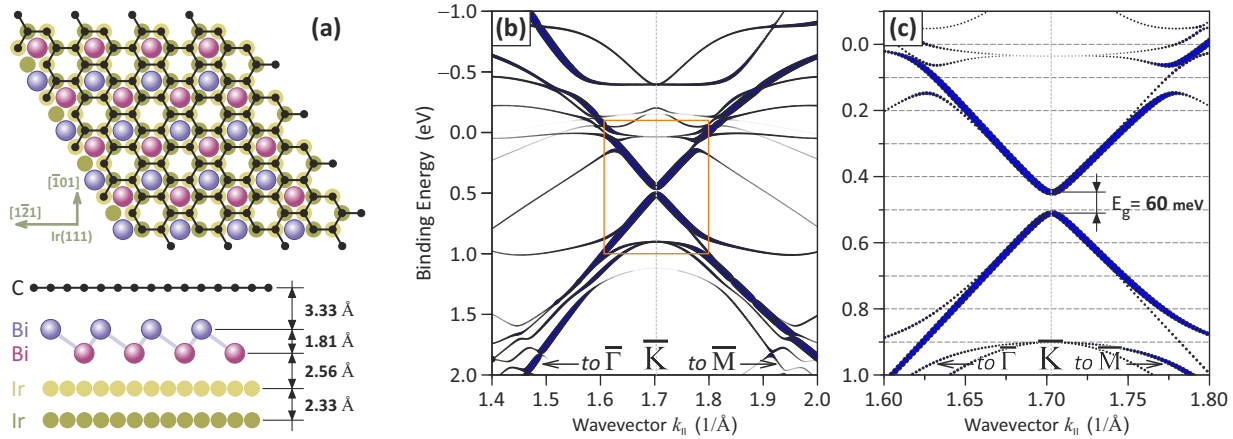

FIG. 8: Density functional theory study of graphene/Ir(111) intercalated with Bi in the form of a honeycomb-shaped buckled layer (bismuthene). This structure creates a band gap at the Dirac point as large as $E_g \sim 60$ meV. (a) Structural model of graphene/Ir(111) intercalated with bismuthene shown as top view (upper panel) and side view (lower panel, view direction is along Ir[1$\bar{2}$1]). (b) Large-scale band structure of graphene/bismuthene/Ir(111) near $\overline{\mathrm{K}}$ traced along $\overline{\Gamma}-\overline{\mathrm{K}}-\overline{\mathrm{M}}$. (c) Zoom of the area marked in (b) by orange rectangle shows the gapped Dirac cone in greater detail. Doubling of bands seen in (c) as well as symmetric occurrence of the band structure relative to $\mathbf{k}_{\parallel}$=1.7 Å^{-1} in (b) arise due to overlap of $\overline{\mathrm{K}}$ and $\overline{\mathrm{K}'}$ valleys backfolded on $\overline{\Gamma}$ as a result of the $(\sqrt{3}\times\sqrt{3})$ $R30^{\circ}$ hexagonal superlattice of the graphene-bismuthene heterostructure.

to what we see in our STM data. At the same time the lattice mismatch between graphene and non-compressed bismuthene should lead to a moiré pattern with a very long period of $\sim$ 140 Å, which would be unobservable by LEED due to its limited resolution.

Fig. 8(b) reports calculated band structure around $\overline{\mathrm{K}}$ in $\overline{\Gamma}-\overline{\mathrm{K}}-\overline{\mathrm{M}}$ direction of graphene Brillouin zone. The symmetric occurrence of the bands is due to backfolding of both $\overline{\mathrm{K}}$ and $\overline{\mathrm{K}'}$ graphene valleys on $\overline{\Gamma}$. This effect is characteristic of $(n\sqrt{3}\times n\sqrt{3})$ graphene superstructures [55, 56]. To facilitate a comparison with the experimental data we calculate spectral weights for each point (reflected by the size of the markers) by unfolding to the primitive Brillouin zone of graphene [36, 37], weights were additionally scaled according to the contribution of C p_z orbitals. The magnification in Fig. 8(c) shows a band gap $E_g \sim 60$ meV and n-doping with $E_D \sim 0.5$ eV, close to the experimentally observed value of ~ 0.4 eV [Figure 2(e)]. The calculated atomic structure as well as the band gap and the doping level are in good agreement with the results obtained in Ref. [57] ($E_g \sim 73$ meV, $E_D \sim 0.5$ eV), where DFT calculations were performed for graphene/bismuthene heterostructure with a similar geometry (structure "ZA-h") and taking into account the spin-orbit interaction. Our band structure calculations with SOC included also showed only a small change in the band gap value from 60 meV to around 50 meV (see Figure S8 of the supplemental material). The small difference in E_g demonstrates that spin-orbit interaction may have only a minor influence on the size of the band gap and cannot be its primary origin, in line with our spin-resolved ARPES results.

The band gap in the calculated band structure of graphene/bismuthene/Ir(111) also cannot be explained by a simple *A*-*B* sublattice symmetry breaking as A and B sites have identical local structure up to a rotation. This effect can appear if there are changes in the hopping terms in the graphene hexagons located directly above the buckled Bi atoms of bismuthene structure.

Considering the real graphene/Bi/Ir(111) realized in our experiment, the nature of the gap can be treated as rather complex, as long as precise atomic arrangement of Bi under graphene is unknown and therefore cannot be properly accounted in the computational model. Apart from the anticipated *A*-*B*-sublattice asymmetry, E_g may contain additional contributions from other mechanisms, e.g. the hexagonal distortion mentioned above.

For the sake of saving computational time in all graphene/Bi/Ir structures tested above, the lattice constants were adjusted to fit these structures in relatively small supercells. The modified periodicity of Ir substrate could have only an indirect effect on the band structure of graphene through the layer of intercalated bismuth and we expect only a minor change in the calculated band gap of graphene. However, such adjustments also inevitably lead to some degree of strain induced in the bismuthene layer.

Even though in our DFT simulations of several feasible atomic models the bismuthene was the most promising structural phase of intercalated Bi providing a gapped Dirac cone comparable to the experiment, we cannot unambiguously conclude whether the HD-phase of Bi has indeed this structure, although our core-level XPS spectroscopy allows to estimate that the concentration of intercalated Bi is consistent with the presence of bilayer. Further structural studies involving e.g. grazing incidence X-ray diffraction or photoelectron diffraction would be helpful.

V. SUMMARY

In summary, we have synthesized a previously unreported structural phase of Bi-intercalated graphene on Ir(111) characterized by high density of the Bi interlayer and studied its electronic and structural properties by means of LEED, spin-resolved ARPES and STM. Intercalated Bi decouples graphene from the Ir(111) and efficiently screens the signal from the Ir substrate in the photoemission experiment. The band structure of such Bi-intercalated graphene was found to be nearly ideal. It reveals no features characteristic of the pristine graphene on Ir(111) such as electronic hybridization between graphene and Ir, moiré pattern and *umklapp*-induced band replicas of the Dirac cone. The only deviations from the freestanding state found in the experiment are a minor n-type charge doping ($E_{\mathrm{D}} \sim E_{\mathrm{F}} - 0.4$ eV) and a relatively small band gap ($E_g \sim 0.19$ eV).

Our microscopic study of the structure reveals a nearly complete elimination of the original Ir-induced moiré pattern and flattening of the graphene layer upon intercalation of Bi. Atomically resolved STM also reveals a graphene lattice with rather weak A-B sublattice asymmetry, as compared to pristine graphene/Ir(111).

We discuss different possible origins of the band gap in Bi-intercalated graphene. Using spin-resolved photoemission we reveal a fully spin degenerate Dirac cone and therefore exclude spin-orbit interaction as origin of the gap. Based on the analysis of the Brillouin-zone-selection effect in the angular distribution of photoemission intensity from the Dirac cone, we conclude on A-B asymmetry as one of the possible origins of the band gap at the Dirac point in Bi-intercalated graphene on Ir(111).

Systematic investigation of the band structure for various concentrations of intercalated Bi reveals the possibility of fine control over the band gap in the Dirac cone of graphene within ± 25 meV by tuning the Bi coverage.

Our findings indicate that the gap is not due to spin-orbit interaction as recently proposed for Pb-intercalated graphene on Pt(111) [20] and therefore is not suited to host quantum spin Hall states.

Aiming to resolve the atomic structure of the high-density phase of intercalated bismuth we performed an extensive DFT analysis of feasible arrangements of Bi atoms at the graphene-Ir(111) interface. Simulations revealed only one Bi structure capable to open a sizeable gap of 0.06 eV which is comparable to the experimentally observed value $E_g \sim 0.19$ eV at least by the order of magnitude. This structure was identified as *bismuthene*. Our results indicate that intercalation of graphene with Bi could be promising for synthesis of a 2D graphene-bismuthene heterostructure.

Acknowledgments

Financial support from SPP 1459 of the Deutsche Forschungsgemeinschaft and from the Impuls- und Vernetzungsfonds der Helmholtz Gemeinschaft under Grants No. HRJRG-408 and HRSF-0067 is gratefully acknowledged.

[1] K. V. Emtsev, F. Speck, T. Seyller, L. Ley, and J. D. Riley, Phys. Rev. B **77**, 155303 (2008).
[2] G. R. Yazdi, T. Iakimov, and R. Yakimova, Crystals **6**, 53 (2016).
[3] A. N. Chaika, O. V. Molodtsova, A. A. Zakharov, D. Marchenko, J. Sánchez-Barriga, A. Varykhalov, I. V. Shvets, and V. Y. Aristov, Nano Res. **6**, 562 (2013).
[4] M. Batzill, Surf. Sci. Rep. **67**, 83 (2012).
[5] A. Varykhalov, M. R. Scholz, T. K. Kim, and O. Rader, Phys. Rev. B **82**, 121101 (2010).
[6] A. Varykhalov, J. Sánchez-Barriga, A. M. Shikin, C. Biswas, E. Vescovo, A. Rybkin, D. Marchenko, and O. Rader, Phys. Rev. Lett. **101**, 157601 (2008).
[7] D. Marchenko, A. Varykhalov, M. R. Scholz, G. Bihlmayer, E. I. Rashba, A. Rybkin, A. M. Shikin, and O. Rader, Nat. Commun. **3**, 1232 (2012).
[8] Y. Zhang, Y. Zhang, D. Ma, Q. Ji, W. Fang, J. Shi, T. Gao, M. Liu, Y. Gao, Y. Chen, et al., Nano Res. **6**, 887 (2013).
[9] L. Meng, R. Wu, H. Zhou, G. Li, Y. Zhang, L. Li, Y. Wang, and H.-J. Gao, Appl. Phys. Lett. **100**, 083101 (2012).
[10] N. I. Verbitskiy, A. V. Fedorov, G. Profeta, A. Stroppa, L. Petaccia, B. Senkovskiy, A. Nefedov, C. Wöll, D. Y. Usachov, D. V. Vyalikh, et al., Sci. Rep. **5**, 17700 (2015).
[11] A. Varykhalov, W. Gudat, and O. Rader, Adv. Mater. **22**, 3307 (2010).
[12] C. Weeks, J. Hu, J. Alicea, M. Franz, and R. Wu, Phys. Rev. X **1**, 021001 (2011).
[13] A. M. Shikin, A. G. Rybkin, D. Marchenko, A. A. Rybkina, M. R. Scholz, Oliver Rader, and A. Varykhalov, New J. Phys. **15**, 013016 (2013).
[14] E. V. Zhizhin, A. Varykhalov, A. G. Rybkin, A. A. Rybkina, D. A. Pudikov, D. Marchenko, J. Sánchez-Barriga, I. I. Klimovskikh, G. G. Vladimirov, O. Rader, et al., Carbon **93**, 984 (2015).
[15] Y. Li, P. Tang, P. Chen, J. Wu, B.-L. Gu, Y. Fang, S. B. Zhang, and W. Duan, Phys. Rev. B **87**, 245127 (2013).
[16] E. I. Rashba, Phys. Rev. B **79**, 161409 (2009).

[17] M. Krivenkov, E. Golias, D. Marchenko, J. Sánchez-Barriga, G. Bihlmayer, O. Rader, and A. Varykhalov, 2D Mater. **4**, 035010 (2017).
[18] P. Rakyta, A. Kormányos, and J. Cserti, Phys. Rev. B **83**, 155439 (2011).
[19] A. Varykhalov, J. Sánchez-Barriga, D. Marchenko, P. Hlawenka, P. S. Mandal, and O. Rader, Nat. Commun. **6**, 7610 (2015).
[20] I. I. Klimovskikh, M. M. Otrokov, V. Y. Voroshnin, D. Sostina, L. Petaccia, G. Di Santo, S. Thakur, E. V. Chulkov, and A. M. Shikin, ACS Nano **11**, 368 (2017).
[21] C. L. Kane and E. J. Mele, Phys. Rev. Lett. **95**, 146802 (2005).
[22] J. Warmuth, A. Bruix, M. Michiardi, T. Hänke, M. Bianchi, J. Wiebe, R. Wiesendanger, B. Hammer, P. Hofmann, and A. A. Khajetoorians, Phys. Rev. B **93**, 165437 (2016).
[23] D. Marchenko, J. Sánchez-Barriga, M. R. Scholz, O. Rader, and A. Varykhalov, Phys. Rev. B **87**, 115426 (2013).
[24] I. Pletikosić, M. Kralj, P. Pervan, R. Brako, J. Coraux, A. T. N'Diaye, C. Busse, and T. Michely, Phys. Rev. Lett. **102**, 056808 (2009).
[25] S. Rusponi, M. Papagno, P. Moras, S. Vlaic, M. Etzkorn, P. M. Sheverdyaeva, D. Pacilé, H. Brune, and C. Carbone, Phys. Rev. Lett. **105**, 246803 (2010).
[26] J. Sánchez-Barriga, A. Varykhalov, D. Marchenko, M. R. Scholz, and O. Rader, Phys. Rev. B **85**, 201413 (2012).
[27] H. Vita, S. Böttcher, K. Horn, E. N. Voloshina, R. E. Ovcharenko, T. Kampen, A. Thissen, and Y. S. Dedkov, Sci. Rep. **4**, 5704 (2014).
[28] A. Stöhr, S. Forti, S. Link, A. A. Zakharov, K. Kern, U. Starke, and H. M. Benia, Physical Review B **94**, 085431 (2016).
[29] J. C. F. M. Warmuth, Master's thesis, University of Hamburg (2014).
[30] A. Varykhalov, O. Rader, and W. Gudat, Phys. Rev. B **72**, 115440 (2005).
[31] G. Kresse and J. Hafner, Phys. Rev. B **47**, 558 (1993).
[32] P. E. Blöchl, Phys. Rev. B **50**, 17953 (1994).
[33] J. P. Perdew, K. Burke, and M. Ernzerhof, Phys. Rev. Lett. **77**, 3865 (1996).
[34] H. J. Monkhorst and J. D. Pack, Phys. Rev. B **13**, 5188 (1976).
[35] S. Grimme, J. Comput. Chem. **27**, 1787 (2006).
[36] V. Popescu and A. Zunger, Phys. Rev. B **85**, 085201 (2012).
[37] Q. Zheng, *VASP band unfolding*, URL `https://github.com/QijingZheng/VaspBandUnfolding`.
[38] A. T. N'Diaye, T. Gerber, C. Busse, J. Mysliveček, J. Coraux, and T. Michely, New J. Phys. **11**, 103045 (2009).
[39] F. Jean, T. Zhou, N. Blanc, R. Felici, J. Coraux, and G. Renaud, Phys. Rev. B **91**, 245424 (2015).
[40] A. Varykhalov, D. Marchenko, M. R. Scholz, E. D. L. Rienks, T. K. Kim, G. Bihlmayer, J. Sánchez-Barriga, and O. Rader, Phys. Rev. Lett. **108**, 066804 (2012).
[41] M. Kralj, I. Pletikosić, M. Petrović, P. Pervan, M. Milun, A. T. N'Diaye, C. Busse, T. Michely, J. Fujii, and I. Vobornik, Phys. Rev. B **84**, 075427 (2011).
[42] E. L. Shirley, L. J. Terminello, A. Santoni, and F. J. Himpsel, Phys. Rev. B **51**, 13614 (1995).
[43] A. Bostwick, T. Ohta, J. L. McChesney, K. V. Emtsev, T. Seyller, K. Horn, and Eli Rotenberg, New J. Phys. **9**, 385 (2007).
[44] E. Starodub, A. Bostwick, L. Moreschini, S. Nie, F. E. Gabaly, K. F. McCarty, and E. Rotenberg, Phys. Rev. B **83**, 125428 (2011).
[45] C. L. Kane and E. J. Mele, Phys. Rev. Lett. **95**, 226801 (2005).
[46] G. M. Rutter, J. N. Crain, N. P. Guisinger, T. Li, P. N. First, and J. A. Stroscio, Science **317**, 219 (2007).
[47] G. Sclauzero and A. Pasquarello, Phys. Rev. B **85**, 161405 (2012).
[48] R. Balog, B. Jørgensen, L. Nilsson, M. Andersen, E. Rienks, M. Bianchi, M. Fanetti, E. Lægsgaard, A. Baraldi, S. Lizzit, et al., Nat. Mater. **9**, 315 (2010).
[49] P. R. Wallace, Phys. Rev. **71**, 622 (1947).
[50] D. P. DiVincenzo and E. J. Mele, Phys. Rev. B **29**, 1685 (1984).
[51] R. Skomski, P. A. Dowben, M. S. Driver, and J. A. Kelber, Mater. Horiz. **1**, 563 (2014).
[52] I. Gierz, J. Henk, H. Höchst, C. R. Ast, and K. Kern, Phys. Rev. B **83**, 121408 (2011).
[53] A. Bostwick, F. Speck, T. Seyller, K. Horn, M. Polini, R. Asgari, A. H. MacDonald, and E. Rotenberg, Science **328**, 999 (2010).
[54] I. I. Naumov and P. Dev, Phys. Rev. Research **2**, 023157 (2020).
[55] Y. Ren, X. Deng, Z. Qiao, C. Li, J. Jung, C. Zeng, Z. Zhang, and Q. Niu, Phys. Rev. B **91**, 245415 (2015).
[56] S. Casolo, R. Martinazzo, and G. F. Tantardini, J. Phys. Chem. C **115**, 3250 (2011).
[57] Z. Li and Z. Zhang, Phys. Status Solidi RRL p. 2000131 (2020).

Supplementary Information for the Manuscript

ORIGIN OF THE BAND GAP IN Bi-INTERCALATED GRAPHENE ON Ir(111)

Maxim Krivenkov[1,2], Dmitry Marchenko[1], Jaime Sánchez-Barriga[1], Evangelos Golias[1], Oliver Rader[1] and Andrei Varykhalov[1,*]

[1] *Helmholtz-Zentrum Berlin für Materialien und Energie, Elektronenspeicherring BESSY II, Albert-Einstein-Str. 15, 12489 Berlin, Germany*

[2] *Institut für Physik und Astronomie, Universität Potsdam, Karl-Liebknecht-Str. 24/25, 14476 Potsdam, Germany*

[*] *Corresponding author: andrei.varykhalov@helmholtz-berlin.de*

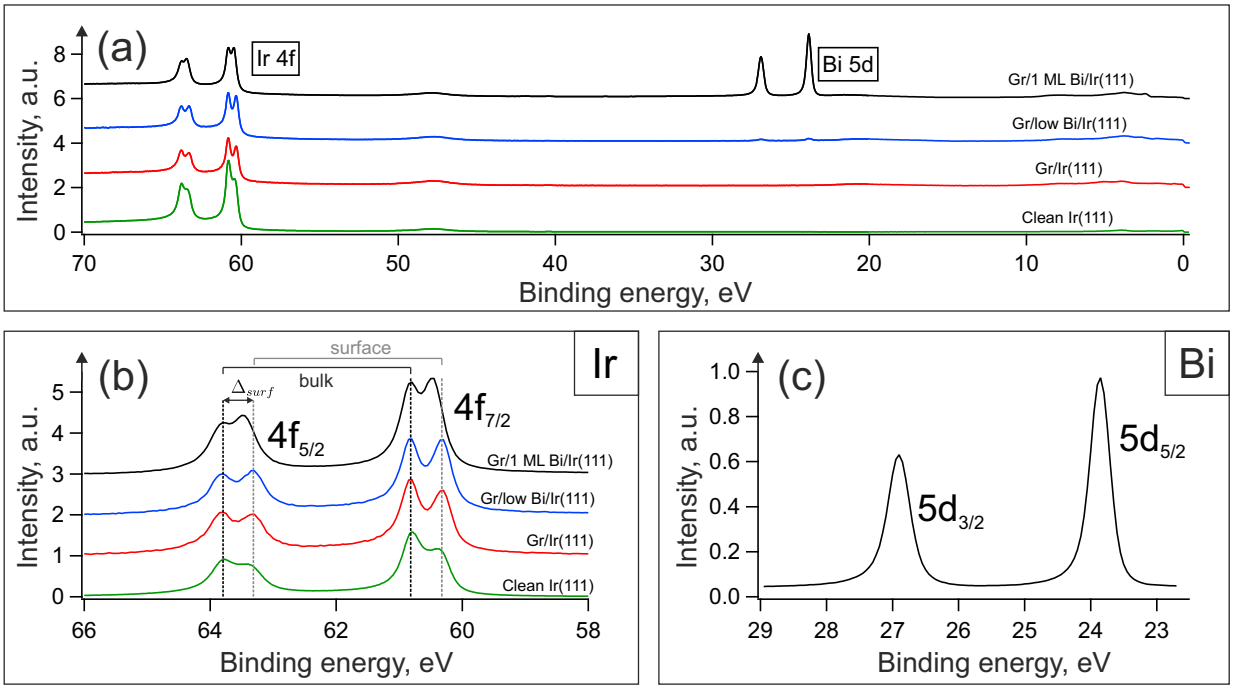

FIGURE S1. Core level spectroscopy of graphene/Bi/Ir(111) at different stages of sample preparation (from bottom to top): clean Ir(111), graphene/Ir(111), sample with low concentration of intercalated Bi and fully intercalated sample (1 ML of Bi). For intercalation Bi was deposited on hot graphene/Ir(111) maintained at 750 K for 30 min. All spectra were measured with photon energy $h\nu = 120$ eV. (a) Overview spectra. (b) Close-up of Ir 4f CLs with Shirley background subtracted (relative intensities are not to scale), positions of bulk and surface (interface) components are shown with brackets on top. The energy shift Δ_{surf} of the surface component relative to the bulk one first increases from $\Delta_{surf} = 0.43$ eV for Ir(111) to 0.53 eV for graphene/Ir(111) and after Bi intercalation decreases to 0.38 eV. (c) Close-up of Bi 5d CLs for fully intercalated sample.

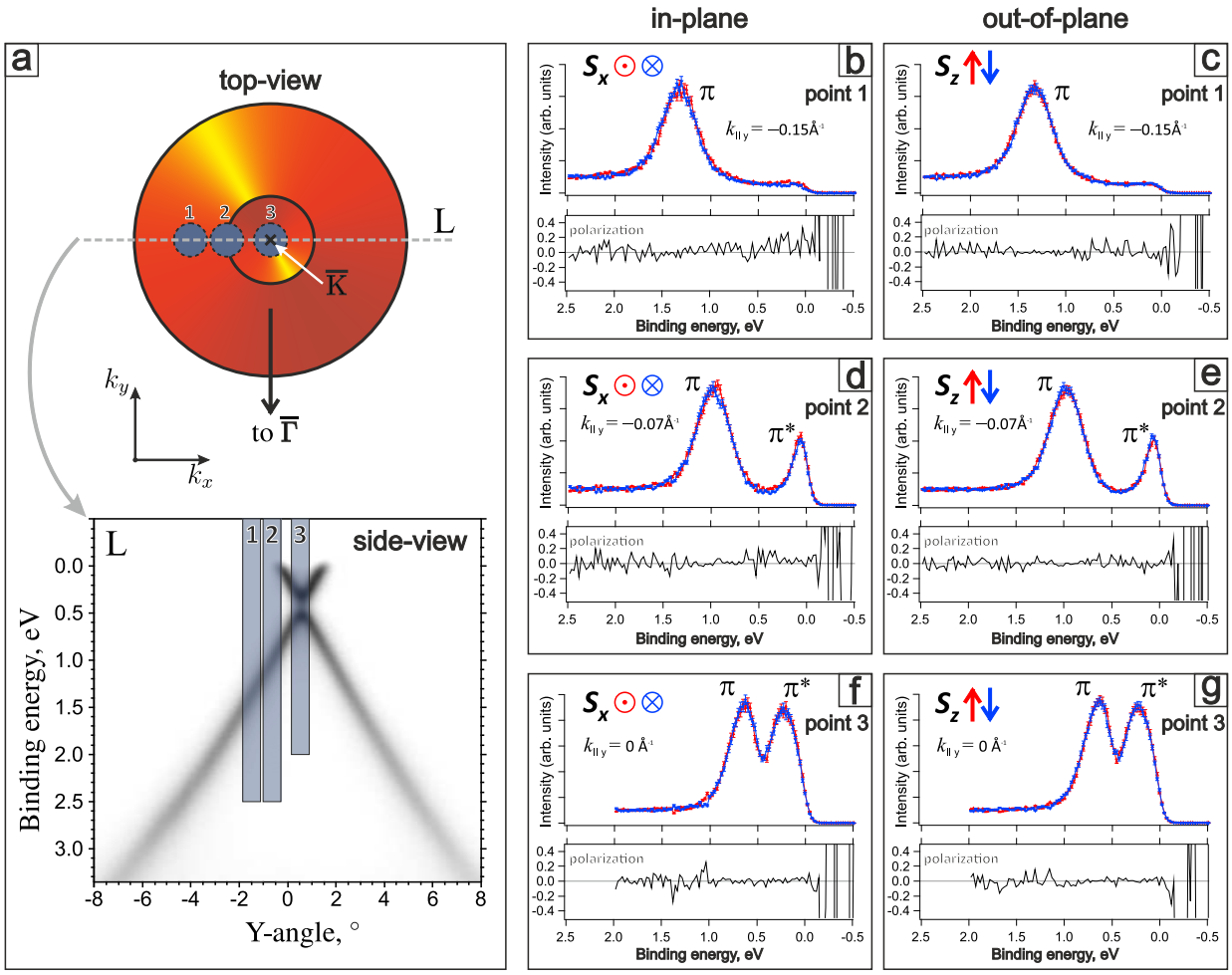

FIGURE S2. Characterization of Dirac cone of HD-phase of Bi-intercalated graphene on Ir(111) by spin- and angle-resolved photoemission. Spin-resolved spectra of 3D projections of spins were acquired at points 1, 2 and 3 as shown in (a). Upper panel in (a) displays location of these points in ($\mathbf{k}_{\parallel,x}$, $\mathbf{k}_{\parallel,y}$) plane projected on a schematic top-view of the Dirac cone. Lower panel in (a) shows location of these points (EDC spectra) within E(Y) dispersion cut L through $\overline{\mathrm{K}}$ point. Dispersion is shown as raw data (energy vs. emission angle Y). (b–f) Corresponding spin-polarizations and spin-resolved EDC spectra acquired at points 1, 2 and 3. Only projections S_x and S_z, revealing in-plane Rashba-type and out-of-plane hedgehog-type spin orientations, respectively, are relevant and shown. Point 1 (b,c) reveals spin polarization of valence band π at $\mathbf{k}_{\parallel,y}$=−0.15 Å^{-1} away from $\overline{\mathrm{K}}$. Point 2 (d,e) reveals polarization of both valence and conduction bands π and π^* at $\mathbf{k}_{\parallel,y}$=−0.07 Å^{-1}. Point 3 (d,e) reports spin texture of the band gap precisely at the $\overline{\mathrm{K}}$ point. Dirac cone is spin degenerate everywhere.

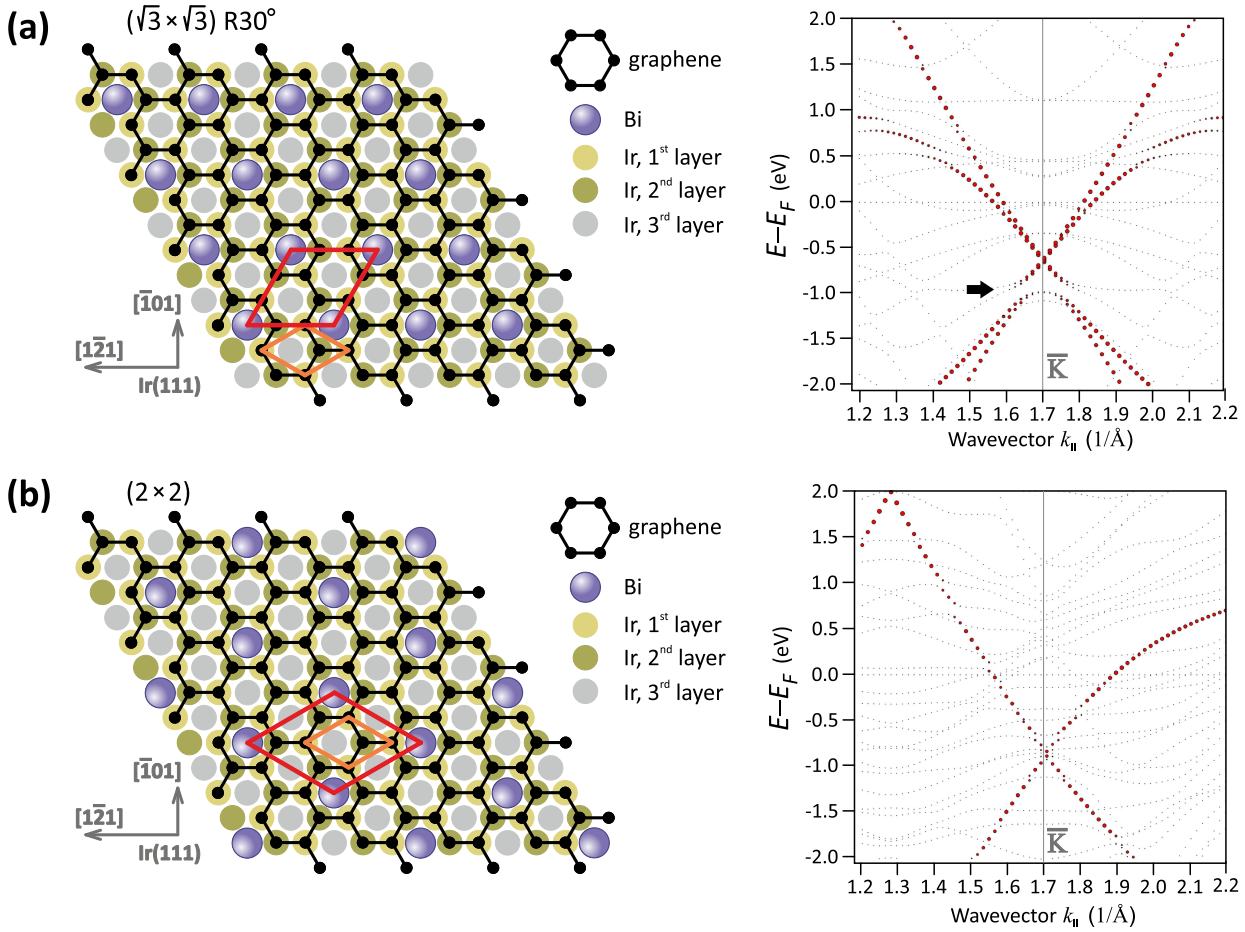

FIGURE S3. Band structure of the most realistic (from general symmetry considerations) structures of Bi under graphene on Ir(111) obtained by density functional theory (DFT): $(\sqrt{3} \times \sqrt{3})$ $R30°$ (a) and (2×2) (b). Left panels display atomic structures used in the calculations. Red and orange rhombus denote surface lattice unit cells of Bi superstructures and graphene, respectively. Right panels display regions of calculated band structures near $\overline{\mathrm{K}}$ of the graphene SBZ and show Dirac cones. For $(\sqrt{3} \times \sqrt{3})$ $R30°$ only a hybridization gap ~ 0.3 eV below the Dirac energy is seen (black arrow). The Dirac point itself, however, remains intact for both structural phases of Bi.

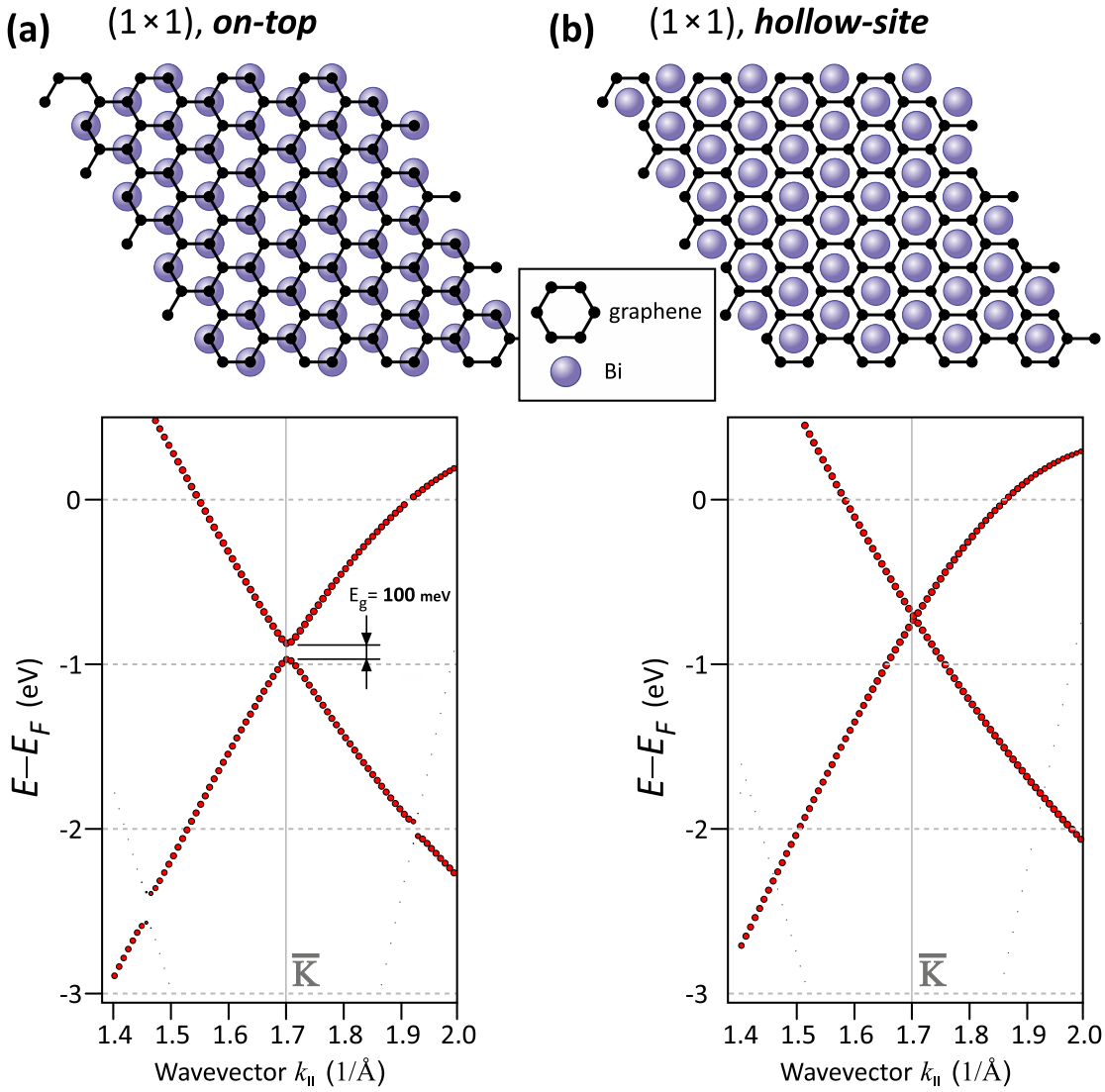

FIGURE S4. Test of ultimate sublattice symmetry breaking in graphene by (1×1) structures of Bi. Ir(111) substrate is neglected. (a) In *on-top* configuration (when C atoms from one graphene sublattice reside exactly above Bi atoms and C atoms from the other sublattice are located in hollow positions) a band gap as large as $\sim$ 100 meV appears. This is, however, smaller than the experimentally observed value $E_g \sim 190$ meV. (b) When the system is switched to the energetically more favorable *hollow-site* configuration (all carbon atoms are in hollow positions and Bi atoms are placed at the centers of graphene hexagons) the band gap in the Dirac cone disappears. We emphasize, that both presented (1×1) stuctures are unphysical and cannot exist in reality because of large diameters of Bi atoms. They are used only as example.

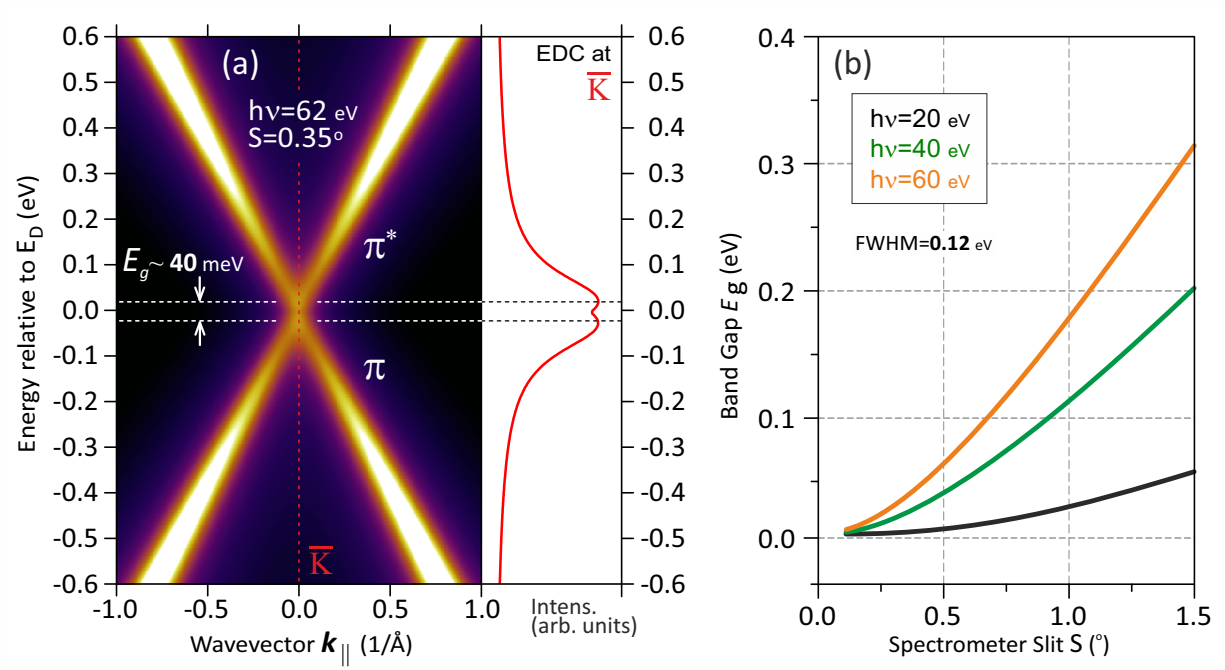

FIGURE S5. (a) Simulated ARPES spectrum of Dirac cone accounting for finite angular resolution of the analyzer in the direction perpendicular to the analyzer slit. Simulation is performed for the band structure of ideal graphene given by a tight-binding model [1]. Steep dispersion of Dirac bands in combination with highly anisotropic distribution of photoelectron intensity within constant energy surfaces caused by interference effects [2] results in the occurrence of artificial band gaps at the Dirac point. For the experimental angular resolution of 0.35° and photon energy of 62 eV the artificial band gap (E_g) is about 40 meV; (b) Diagram shows evolution of the band gap E_g with deteriorating angular resolution (enlargement of spectrometer slit S) calculated for three different photon energies (20, 40 and 60 eV). In the course of simulation photoemission peak of Dirac band was modeled by EDC Lorentzian with FHWM=120 meV (empirical value). A detailed report on ARPES simulations is to be published [3].

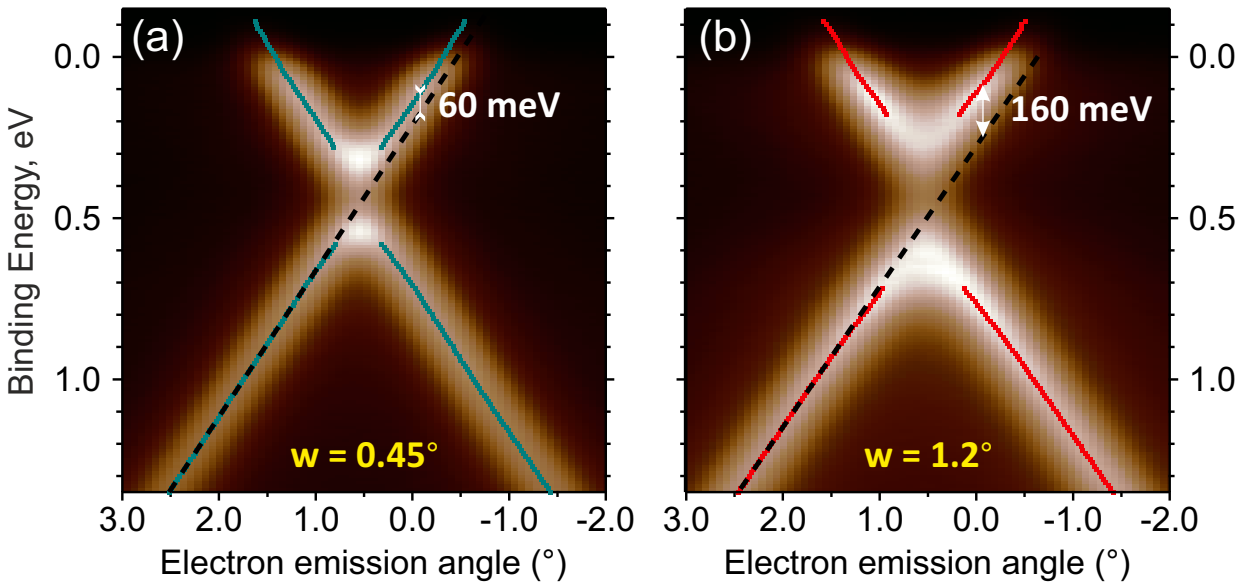

FIGURE S6. Experimental ARPES spectrum of the Dirac cone in graphene/Bi/Ir(111) measured using analyzer entrance slits of different width w: (a) $w = 0.45°$; (b) $w = 1.2°$. Dots show the apparent dispersion of the Dirac cone, extracted by fitting of the momentum distribution curves with Lorentzian profiles, each dot marks a peak position. The black dashed lines are a linear fit of the bottom left part of the dispersions (extended towards the Fermi level). One can directly see that for larger slit width not only the apparent band gap significantly increased, but also the apparent energy shift between the lower and upper parts of the cone.

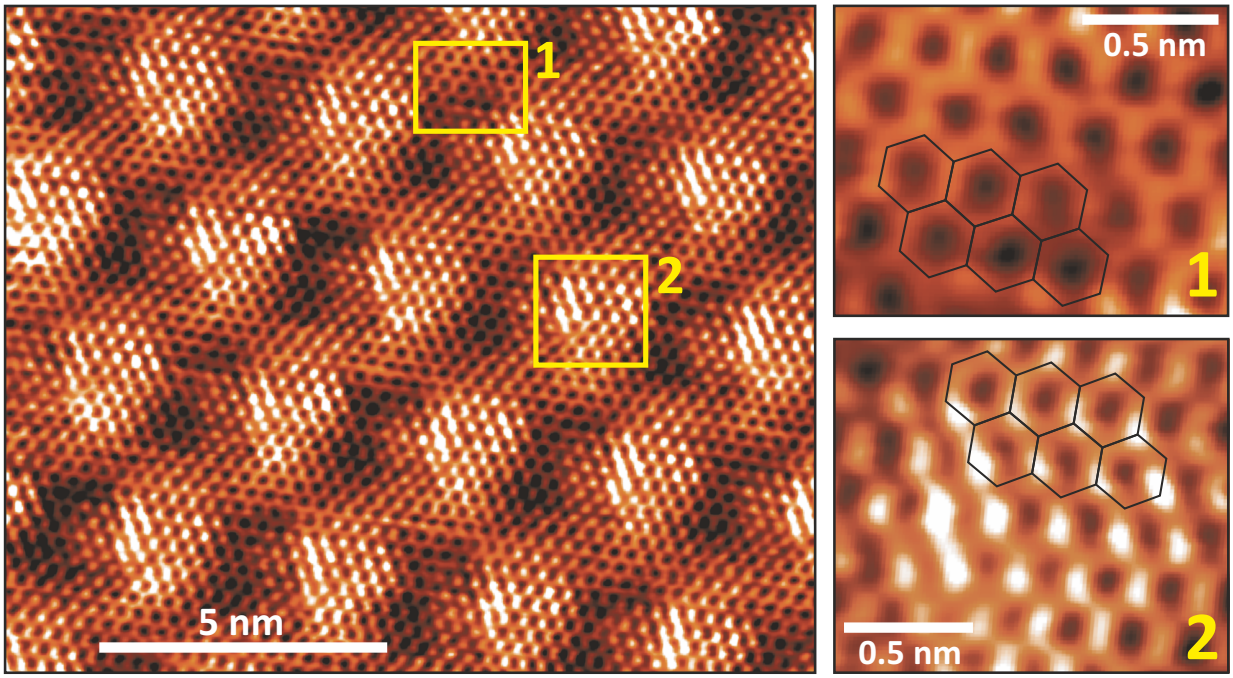

FIGURE S7. STM image of moiré-patterned graphene/Ir(111) with atomic resolution. Measurement parameters: bias voltage $V_t = +2$ mV, tunneling current $I_t = 34$ nA. Panels at right show zoom of the areas 1 and 2 with graphene lattice superimposed. While area 1 exhibits equivalent appearance of graphene sublattices, area 2 reveals strong local A-B asymmetry manifested by strongly enhanced signal from one of the sublattices.

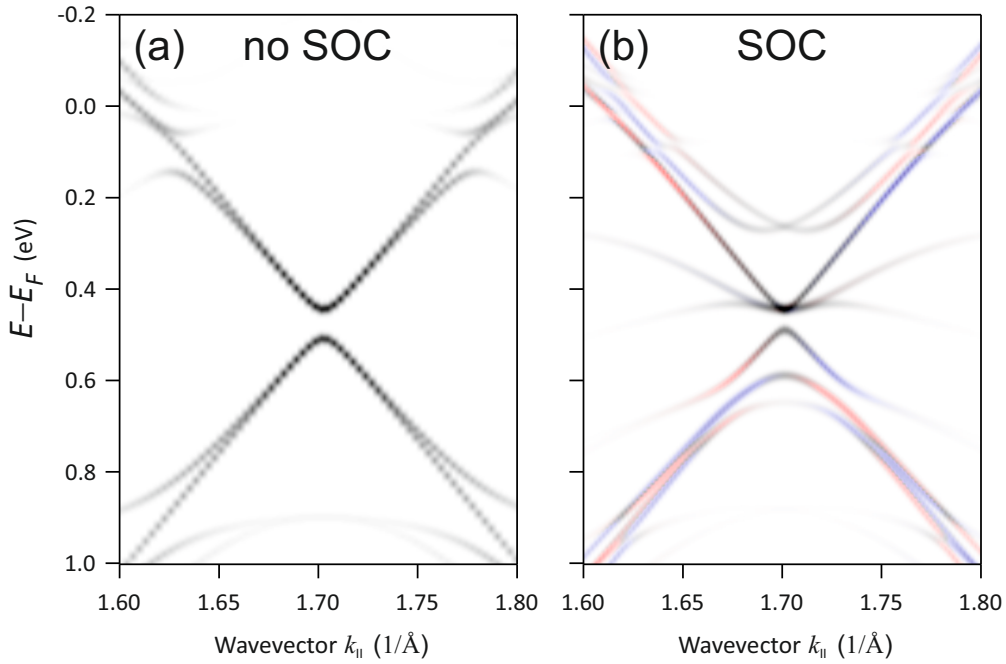

FIGURE S8. Calculated band structures for graphene/bismuthene/Ir(111) near $\overline{\mathrm{K}}$ in direction $\overline{\Gamma} - \overline{\mathrm{K}} - \overline{\mathrm{M}}$ of the Brillouin zone of graphene (a) without spin-orbit coupling (SOC) and (b) with SOC included. Band structures are projected on C p_z orbitals of graphene. Red and blue colors in panel (b) reflect the magnitude and direction of spin projection perpendicular to the plane of the image.

[1] P. R. Wallace, "The band theory of graphite," Phys. Rev. **71**, 622–634 (1947).

[2] Aaron Bostwick, Taisuke Ohta, Jessica L. McChesney, Konstantin V. Emtsev, Thomas Seyller, Karsten Horn, and Eli Rotenberg, "Symmetry breaking in few layer graphene films," New J. Phys. **9**, 385 (2007).

[3] Andrei Varykhalov et al., "Artificial band gaps and angular resolution effects in angle-resolved photoemission from flat and rippled graphene," In preparation.